Astron. Astrophys. 310, 8–30 (1996)

ASTRONOMY AND ASTROPHYSICS

The ESO Nearby Abell Cluster Survey

I. Description of the dataset and definition of physical systems*,**

P. Katgert[1], A. Mazure[2], J. Perea[3], R. den Hartog[1], M. Moles[3], O. Le Fèvre[4], P. Dubath[5], P. Focardi[6], G. Rhee[7], B. Jones[8], E. Escalera[9,10], A. Biviano[1,11], D. Gerbal[4,11], and G. Giuricin[9,12]

[1] Sterrewacht Leiden, The Netherlands
[2] Laboratoire d'Astronomie Spatiale, Marseille, France
[3] Instituto de Astrofísica de Andalucía, CSIC, Granada, Spain
[4] DAEC, Observatoire de Paris, Université Paris 7, CNRS (UA 173), France
[5] Observatoire de Genève, Switzerland & Lick Observatory, Univ. of California, Santa Cruz, USA
[6] Dipartimento di Astronomia, Università di Bologna, Italy
[7] Department of Physics, University of Nevada, Las Vegas, USA
[8] Nordita, Copenhagen, Denmark
[9] Dipartimento di Astronomia, Università di Trieste, Italy
[10] Royal Observatory, Edinburgh, UK
[11] Institut d'Astrophysique de Paris, France
[12] SISSA, Trieste, Italy

Received 22 December 1994 / Accepted 2 October 1995

Abstract. We describe the results of the ESO Key-programme on "Structure and Dynamics of Rich Galaxy Clusters" (which we will henceforth refer to as the ESO Nearby Abell Cluster Survey - or ENACS). We discuss the sample of clusters for which data were obtained, and the observational programme of spectroscopy and photometry that we carried out. The final database contains a total of 5634 galaxies in the directions of 107 clusters from the catalogue by Abell, Corwin and Olowin 1989 (ACO hereafter) with richness $R \geq 1$ and mean redshifts $z \leq 0.1$. For 4465 galaxies the redshift is based solely on absorption lines, for 586 galaxies it is based on both absorption and emission lines, while for the remaining 583 galaxies the redshift is based exclusively on one or more emission lines. For 5615 galaxies an R_{25} magnitude was obtained. We discuss in some detail the methods of observation and analysis and determine the quality and reliability of the data from independent, repeated measurements. All absorption-line redshifts with a low S/N-ratio of the peak in the correlation function have been judged on plausibility by combined visual inspection of spectrum and correlation function. This has led to an empirically determined overall reliability of the 5634 accepted redshifts of 0.98.

We discuss various methods for defining the compact, physically relevant systems in the 107 'pencil-beam' surveys. We have chosen to apply a fixed velocity gap to separate galaxies that do not form part of the same system. From the summed distribution of the velocity differences between galaxies adjacent in redshift we conclude that, for the average system in our survey, and for our sampling of the velocity distributions, a velocity gap of 1000 km/s is the optimum one for defining the systems. With this gap size, systems are not broken up into sub-systems, and field galaxies are hardly linked to the systems. We present the mean redshifts of the 220 systems (with at least 4 members) identified in the 107 pencil beam surveys, using a fixed gap of 1000 km/s.

On average, about 75% of the 5634 galaxies are in the largest system found in the direction of the rich Abell cluster candidate. This shows that, within $\approx 1\ h^{-1}$ Mpc of the cluster centre and down to $R \approx 17$, field contamination is not negligible for clusters with $z \lesssim 0.1$. However, about half of the 25% of galaxies outside the largest system belong to a secondary system along the same line of sight.

At the same time, field contamination has produced only a small number of spurious rich clusters within the sample of $R \geq 1$, $z \leq 0.1$ clusters. For about 90 % of the nearby rich Abell cluster candidates studied here we find a redshift system that either contains more than half of the total number of redshifts, or that has at least two times as many redshifts as the next largest system. Only in about 10% of the cases does an $R \geq 1$, $z \leq 0.1$ entry in the ACO catalogue appear to be the result of a superposition of two almost equally rich (but relatively poorer) systems. Almost all of the rich and relatively nearby

Send offprint requests to: P. Katgert

* Based on observations collected at the European Southern Observatory (La Silla, Chile)

** Table 6 is also available in electronic form at the CDS via anonymous ftp 130.79.128.5

ACO cluster candidates that we studied thus appear to be real rich clusters that represent physical systems.

Key words: galaxies: clusters of – galaxies: redshifts – cosmology: observations – dark matter

1. Introduction

Rich clusters of galaxies have long been recognized as objects that can provide information about important aspects of the physics of large-scale structure formation. Their spatial distribution, their motions with respect to the Hubble flow, and the distribution of their global properties, such as total mass and shape, all hold clues to details of the formation process. Among the latter are the form and amplitude of the spectrum of initial fluctuations on cluster scales, and the average density of the expanding background Universe in which the clusters form (e.g. White 1992, and references therein).

In the central parts of rich clusters, the memory of the initial conditions on sub-cluster scales has most probably been erased completely. On the other hand, the relaxation times outside the cores are definitely longer than a Hubble-time so that (dynamical) structure in the outer parts may contain clues about initial conditions on sub-cluster scales, and about dynamical processes that are important during the collapse of the cluster (e.g. West, Dekel & Oemler 1987). In addition, the central regions of rich clusters are ideal 'laboratories' for the study of the dynamical effects that occur in environments where the galaxy density is very much higher than average. Finally, the present-day distribution of the masses of the cluster galaxies reflects the initial mass function on galaxy scales, modified by the growth and destruction processes that result from encounters between galaxies (e.g. Sarazin 1986).

For several aspects of the study of the properties of rich clusters it suffices to observe a well-chosen set of clusters, without the need to rigorously define a complete sample. However, for many purposes it is essential that the analysis is based on a cluster sample that is statistically complete. Obvious cases include: the determination of the cluster mass function, and the study of the distribution of cluster shapes. In these instances, a useful comparison with model predictions is only possible if the dataset that is used to constrain the models is complete in a well-defined manner, or if its incompleteness can be described with sufficient accuracy.

Complete samples of clusters can at present be defined in two ways. Either one uses optical galaxy catalogues, or high-latitude surveys of X-ray sources to define candidate clusters. In both cases spectroscopic follow-up is required to confirm the reality of the candidate clusters and to find their distances. In the near future it will become possible to use wide-area redshift surveys of galaxies out to considerable distances to define cluster samples in a direct and controlled manner.

Both of the methods presently available to define cluster samples have their disadvantages. Optical cluster catalogues, whether based on visual inspection of survey plates (Abell 1958, and Abell, Corwin & Olowin 1989, hereafter ACO) or on galaxy catalogues generated with automatic scanning machines (Lumsden et al. 1992, Dalton et al. 1992) suffer from superposition effects; i.e. the spatial compactness of the peaks in the projected galaxy distribution is not guaranteed, and has to be confirmed. Moreover, the only parameter with respect to which such a cluster sample can be defined to be complete is apparent richness: the number of member galaxies in a cone with a fixed cross-section at the distance of the cluster in a specified range of apparent magnitude. The relation between richness and a physical property such as total mass is not obvious, so completeness in terms of total mass is much harder to achieve.

The superposition problem hardly exists for cluster samples based on X-ray surveys, because in X-rays the contrast of a cluster with respect to the field is much higher than it is in the galaxy distribution. However, samples of X-ray clusters can be made complete only with respect to X-ray flux. The extraction of a volume-limited sample (as required for several types of argument) requires spectroscopy of member galaxies, which then also yields X-ray luminosities (e.g. Briel and Henry 1993, and Pierre et al. 1994). Even X-ray based cluster samples may not be complete with respect to a physically relevant parameter like total mass, if X-ray luminosity and total mass are not very strongly correlated.

There now exist several extensive redshift surveys of galaxies in clusters in the literature (e.g. Colless & Hewett 1987, Dressler & Shectman 1988, Teague, Carter & Gray 1990, Zabludoff, Huchra & Geller 1990, ZHG hereafter, Malumuth et al. 1992, Guzzo et al. 1992, Dalton et al. 1994). However, these data do not yet allow the construction of a large complete, volume-limited sample of rich clusters with good data on e.g. velocity dispersions, internal structure etc. (even if some of the surveys are complete in one way or another). In this paper we describe an observational project, with the status of an ESO Key-programme, which is aimed at providing good and extensive redshift data for a complete sample of at least 100 rich clusters out to a redshift of about 0.1. In combination with literature data this should yield accurate mean redshifts for well over 100 clusters and meaningful estimates of global velocity dispersion for a large fraction of those. For a subset of between 20 and 30 of the richest clusters, the aim is to obtain at least about 100 redshifts for a detailed analysis of the kinematics of the cluster galaxies, to allow a discussion of the cluster dynamics.

The impact of our programme in this area can be illustrated as follows. A recent compilation by Biviano et al. (1992) of available cluster redshift data in the literature contains 6470 redshifts; hence: the ENACS almost doubles the available number of redshifts in the direction of rich clusters. More importantly: it is the largest homogeneous dataset of redshifts of galaxies in clusters. This is clear from our discussion of the distribution of velocity dispersions for a complete, volume-limited cluster sample (Mazure et al. 1995). In that case more than 80% of the redshifts were contributed by our redshift survey.

In Sect. 2 we describe the cluster sample that we have studied, as well as the definition of the galaxy samples in the di-

rection of these clusters, on which we carried out multi-object spectroscopy. In Sect. 3 we briefly describe the spectroscopic observations, some relevant details of the spectroscopic reduction, and the methods by which we obtained absorption- and emission-line redshifts. In Sect. 4 we discuss the quality and the reliability of the redshift estimates, internally from multiple measurements, and externally from comparison with literature data. In Sect. 5 we describe how we calibrated our photographic photometry with CCD-imaging, and we discuss the quality of the calibration, and the completeness of the redshift surveys. In Sect. 6 we discuss the results of our spectroscopy, from the point of view of the definition of physically relevant redshift systems in our pencil-beam surveys which are centered on target clusters from the ACO catalogue. In Sect. 7 we discuss for our cluster sample the effects of field contamination and superposition. In Sect. 8 we describe the spatial distribution of the clusters, and of the galaxies in the clusters for which the positional selection function is not straightforward. Finally, in Sect. 9 we summarize the most important conclusions.

2. The Cluster sample and the definition of the galaxy samples

2.1. The sample of clusters observed in the ENACS

We designed the ENACS so that it would establish, upon completion and in combination with literature data, a redshift database for an essentially complete sample of Abell clusters with richness $R \geq 1$ out to a redshift z of about 0.1, in the solid angle of 2.55 sr around the South Galactic Pole, defined by $b \leq -30°$ and $-70° \leq \delta \leq 0°$. We included all $R \geq 1$ clusters which, at the start of the project in 1989, either had a spectroscopic redshift $z \leq 0.1$ or had a high probability of having $z \leq 0.1$, in view of their value of m_{10}. As the $m_{10} - z$ relation indicates that most of the clusters with $z \leq 0.1$ have $m_{10} \leq 16.9$, we included all clusters with $m_{10} \leq 16.9$. The width of the $m_{10} - z$ relation implies that one will not have included *all* clusters with $z \leq 0.1$ within this m_{10} limit. To become truly complete out to $z = 0.1$ would have required a (much) fainter limit in m_{10}. Then, however, the scope of the project would have increased unacceptably, while the problem of the lack of a precise completeness limit in redshift would not have disappeared but only have shifted to a higher redshift.

In the course of the project we took into account all information that became available to update the list of clusters still to be observed; i.e. we tried to minimize duplication with work being done elsewhere, and to optimize the yield of our project. We also used the interim results from our observations to improve the definition of the subset of clusters for which we tried to obtain of order 100 redshifts (in our jargon a 'structure cluster'). The 'promotion' of a cluster into the structure-cluster category only took place if the system was sufficiently rich and relatively compact in redshift space, without significant secondary systems at other redshifts.

The full history of the evolution of the definition of the sample is not of interest here. In Sect. 6 the outcome of the process is summarized in the form of a list of the Abell clusters that we have observed, and a global description of the redshift distribution that we measured in the direction of each cluster.

In addition to the clusters in the region defined above, we also observed a few of the clusters in the so-called Shapley concentration (e.g. Bardelli et al. 1994), which is in the Northern galactic hemisphere, around $\alpha = 13^{\rm h}$. In order to make best use of telescope time we added a few 'filler' clusters around $\alpha = 12^{\rm h}$ with $\delta > 0°$.

2.2. Definition of the galaxy samples for spectroscopy

The Southern galaxy catalogues that have been produced in the last few years by groups in the UK, using automatic plate-scanning machines (Lumsden et al. 1992, and Dalton et al. 1992) were not yet available at the beginning of our project. For that reason we had to produce 'special-purpose' galaxy catalogues around the target clusters ourselves. We used the Leiden Observatory *Astroscan* plate-measuring machine (de Vries 1987, Swaans 1981, Van Haarlem et al. 1991) to produce such catalogues. Where possible, we used film copies of the SERC blue survey (IIIa-J emulsion). If that was not possible, the Leiden Observatory glass copies of the first Palomar Sky Survey (103a-E emulsion) were used. Typically, areas of between about 1 and 4 square degrees were scanned at 10 micron ($\approx 0.6''$) resolution. The threshold for object detection was set at a level above sky of between 5 and 7 times the sky noise. For the IIIa-J survey plates this corresponds roughly to a surface brightness cut-off at the 22 mag/arcsec^2 isophote, while for the 103a-E emulsion the cut-off corresponds to about 20.5 mag/arcsec^2.

The catalogues of objects detected above the threshold contain between several and many thousands of entries per cluster. For each of the objects a few basic parameters were determined on-line. The most important ones are the centre-of-gravity position, a photometric parameter $P_{\rm phot}$ (which measures the brightness of the object), and the second moment (size) of the image. The photometric parameter corresponds to 'the amount of silver' in the thresholded part of the image and its logarithm shows an almost linear relation with magnitude (see Sect. 5).

Of course, many objects in the catalogues are not galaxies. In order to eliminate stellar objects as much as possible, we used a two-step scheme. First, we applied an automatic star-galaxy discriminator which uses the second moment of the object in combination with its photometric parameter. Over most of the range in $P_{\rm phot}$ there is a well-defined, very narrow relation between the size and brightness of stellar objects. We fitted a Gaussian to the stellar size distribution in several tens of narrow intervals of brightness. This allowed us to define non-stellar objects as those deviating by more than three standard deviations from the median stellar size for the brightness of the object. Since the stellar locus is very narrow, the fraction of single stars among the non-stellar objects is very small.

However, a non-negligible fraction of the (non-stellar) galaxy candidates are actually double stars. They appear non-stellar because the two images of the stars merge above the detection threshold. On the other hand, bright compact saturated

galaxies can be misclassified as stars. In order to ensure that the galaxy catalogues that we used as the basis of our spectroscopy are not contaminated by stars at the level of more than a few percent and do contain all the bright galaxies, we have visually inspected all objects classified as non-stellar, and all bright objects independent of the classification. This is clearly a method that is less sophisticated than the methods employed for the all-sky catalogues (Heydon-Dumbleton et al. 1989, Maddox et al. 1990). However, visual pattern recognition is quite a powerful tool, as confirmed by the results of our spectroscopy. Contamination of our galaxy catalogues by stars has been limited to an acceptable level of only a few percent.

It must be stressed that, when we selected galaxies for spectroscopic observation, the photographic photometry had not yet been calibrated. The parameter $P_{\rm phot}$ is, however, a sufficiently accurate and monotonically varying function of magnitude. Therefore, we have produced galaxy catalogues with well-defined magnitude limits, by applying a cut-off in $P_{\rm phot}$. This means that we have attempted spectroscopy for all galaxies within circular areas of about 0.5° diameter down to well-defined magnitude limits, which are between 16.5^m and 17.5^m in the R-band. Although the limit varies between clusters, within a cluster the uniformity of the limit over the area of the cluster is quite good, even for clusters for which several fields were observed.

The S/N-ratio in a galaxy spectrum depends primarily on the surface brightness of that part of the galaxy that illuminates the fibre entrance. As the relation between isophotal magnitude and (central) surface brightness of galaxies has an appreciable width, the spectroscopy cannot be (and is not) complete to a limiting isophotal magnitude. Our multi-object spectroscopy is, in principle, complete with respect to central surface brightness within the restriction of the limit in isophotal magnitude that we imposed. The limit in central surface brightness is, however, not very sharp as a result of differences in fibre transmission and in absorption-line strengths.

3. The spectroscopic observations and the determination of redshifts

3.1. The Optopus observations

All spectroscopic observations were carried out with the Optopus multi-fibre spectroscopic facility at the ESO 3.6-m telescope at La Silla (Lund 1986, and Avila et al. 1989). This facility employs an aperture plate at the Cassegrain focus (scale 7.12″/mm), with a diameter of 33′ (or 274 mm). The system uses fibres with 320 micron (or 2.3″) diameter. At one end of the fibre bundle each fibre has its own precision 'connector' which fits tightly into holes drilled in the aperture plate at the positions of the objects to be studied. The other end of the fibre bundle is formed into a linear array of fibres fitted into a connector which positions the fibre ends, which thus replace and define the slit of the Boller & Chivens spectrograph.

In Table 1 we list the relevant instrumental details for the various observing runs. From this Table, some of the modifications that were made to the system during the period over which the observations were made (from September 1989 to October 1993), and which improved its efficiency, can be deduced.

First, the number of fibres increased from 31 to 50 at the beginning of 1990. At the same time a faster camera was installed in the spectrograph. Second, in the fall of 1990 a large fraction of the overhead associated with inserting the 50 fibres in the aperture plate at the telescope was eliminated by the introduction of a second, exchangeable fibre bundle (not visible from Table 1, but very important). This allowed the preparation of an aperture plate during the exposure of the preceding plate. Third, there has been a marked improvement in the properties of the CCD-detectors; our project has benefitted particularly from the decrease of the read-out noise.

The frames were generally exposed for between 60 and 100 minutes, except in the first observing period, when exposure times were generally limited to between 35 and 60 minutes which, with the lower number of fibres (31 instead of 50), causes the observations of September 1989 to be significantly less efficient than the other ones.

In general, atmospheric conditions were good during the exposures. A fair fraction of the exposures was affected by moonlight. In those cases one cannot use an automatic analysis to find the peak in the cross-correlation function (see below), as there frequently is a dominant peak at zero-redshift. Several exposures were carried out during mediocre, and even cloudy, conditions, which affected the S/N-ratios in the galaxy spectra quite badly. This applies in particular to exposures of the clusters A2502, A2933, A3144, A3301 and A3781. As a result, the absence of clear, coherent redshift systems in the data of A2502 and A3144 (see Sect. 6) does not prove conclusively that the target Abell cluster does not exist. We should mention in this context that for none of the rather short exposures from September 1989 such ambiguity exists, because in all clusters that were observed during that run coherent systems were found.

3.2. The accuracy of the positioning of the fibres

In multi-object spectroscopy with aperture plates, the quality of the positioning of the fibres must be ensured in the preparation of the aperture plates, as no changes can be made at the telescope. Because corrections for differential refraction are applied to the object positions, the plate is optimally suited for a particular hour angle, and thus only usable within a window of a few hours around it. The correct positioning of individual fibres is important; not only does it guarantee maximum output, but it also minimizes biases due to possible a-symmetric contributions from galaxy rotation to the systemic velocities.

The positioning of a plate with respect to the sky employs guide stars, which allow one to find the correct telescope pointing position, as well as to align the plate by rotating it. In the original Optopus system, the pointing and rotation were simultaneously fixed by two guide stars. An important improvement resulted from decoupling the two by using a single star (close to the centre of the plate) for pointing, and a set of guide stars near the edge of the plate to control rotation. Only guide stars

Table 1. Details of the instrumental set-up for the Optopus spectroscopy with the 3.6-m telescope.

Observing period	year	CCD format	pixel (μm)	Spectral disp. (Å/mm)	sampl. (Å/pxl)	range (Å)	# fibres
03/09 – 08/09	1989	640×1024	15	133	2.0	3855 – 5880	31
		640×1024	15	172	2.6	3870 – 6510	31
31/03 – 02/04	1990	640×1024	15	130	1.9	3925 – 5860	50
14/09 – 17/09	1990	640×1024	15	130	1.9	3930 – 5865	50
12/10 – 14/10	1990	512×512	27	130	3.5	3925 – 5725	50
02/10 – 08/10	1991	512×512	27	130	3.5	3940 – 5740	50
25/09 – 28/09	1992	512×512	27	130	3.5	3870 – 5670	50
19/10 – 23/10	1992	512×512	27	130	3.5	3850 – 5650	50
14/09 – 16/09	1993	512×512	27	130	3.5	3980 – 5780	50
19/10 – 23/10	1993	512×512	27	130	3.5	3980 – 5780	50

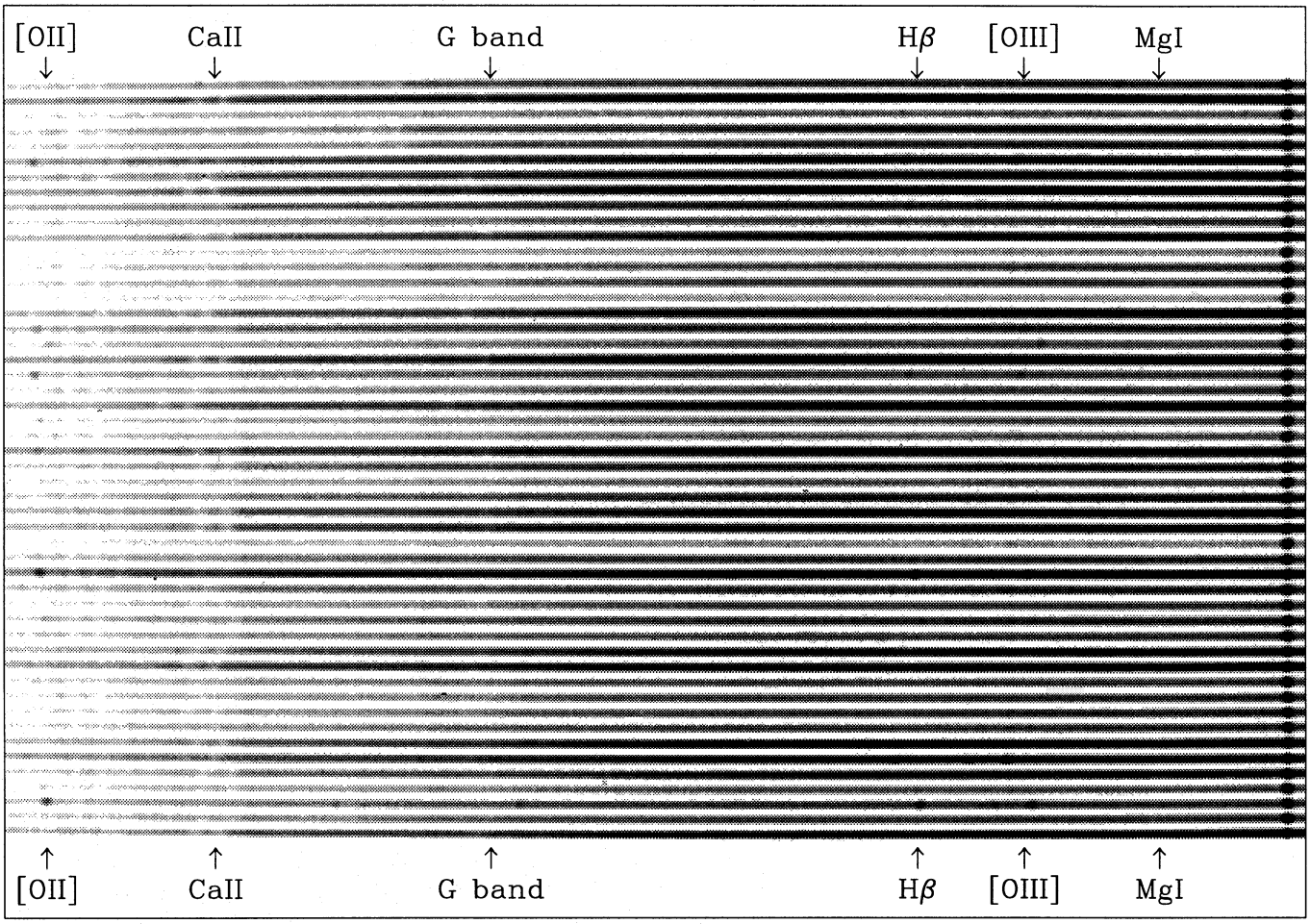

Fig. 1. An example of a CCD frame obtained with the ESO Optopus multi-object spectrograph at the ESO 3.6m telescope. Wavelength increases from left to right. The main absorption and emission features are indicated. At the far right is the sky line at 5577 Å.

with low proper motions (i.e. $\mu < 0.025''$/yr) were used. The pointing errors are estimated to be of the order of at most a few times $0.1''$, while misalignment through rotation does not add more than a few times $0.1''$ at the edge of the plate.

Consistency between the positional systems of guide stars and galaxies is ensured because all positions are derived from the same machine scans. For the mapping of the geometry of the survey Schmidt plates onto the geometry of the 3.6-m Cassegrain focal plane we used the positions of several tens of standard stars. This mapping takes into account the effects of deformation and differential refraction during the exposures of the Schmidt telescope survey plates. From the quality of the standard star fits we estimate that relative positions of the fibres are accurate to within again a few times $0.1''$. Finally, the accuracy of the computer-controlled drilling machine, in combination with the scale of about $7''$/mm at Cassegrain focus, ensures that the mechanical production of the plates does not corrupt the quality of the positioning system.

3.3. The calibration and reduction of the Optopus frames

An exposure with the Optopus system yields a CCD-frame on which about 50 (or 31) parallel, simultaneously recorded spectra are present. As can be seen from Fig. 1 the extraction of the individual spectra does not pose any problems, because adjacent spectra are separated by about 3 non-exposed pixels. The calibration and reduction of the Optopus CCD-frames is in many ways standard. In particular, in the wavelength calibration, the dispersion relation was determined for one of the fibres from the arc-lamp spectra taken before and after each exposure. Subsequently, for the other fibres zero-point shifts were determined using this dispersion relation. The quality of the wavelength calibration was estimated, from the formal quality of the fit (based mostly on between five and ten arc lines) and from the observed wavelengths of (mostly two) sky lines, to be between 0.1 and 0.2 Å.

From the extracted wavelength-calibrated galaxy spectra, cosmic-ray events and emission- and sky-lines were interactively removed. As shown by Lissandrini et al. (1994) it is possible to achieve fairly accurate sky subtraction in multi-fibre spectroscopy by using the strength of one or more sky-lines as a reference. We have monitored the sky brightness by exposing one or two fibres to blank sky in each Optopus exposure. From this we found that the sky brightness is significantly less (over the wavelength range of our observations) than the average brightness, within the fibre aperture, of most of our galaxies. Therefore, we decided not to attempt to subtract the contribution from sky.

Each spectrum was resampled on a regular grid in a logarithmic wavelength scale, as were several template spectra of bright nearby galaxies, as well as of several bright galaxies in the clusters that we investigated, and of stars. Redshifts were determined from cross-correlating the observed galaxy spectrum with a template spectrum, using the methods described by Tonry & Davis (1979). In particular, we also subtracted (before cross-correlation) a polynomial fit to the continuum and apodized the result with a cosine bell to remove the discontinuity between beginning and end of the spectrum. As is well-known, the correlation strength depends very much on the extent to which the object and template spectra agree in detail. After various tests we decided to use a single template to measure redshift values, namely a spectrum of the nucleus of M 31 obtained by Keel at KPNO. We chose this spectrum because it was found to provide the highest *average* correlation strength. Although our use of a single template does not provide maximum correlation strength for each and every galaxy, it does guarantee consistency of redshift estimates between clusters. Because we have visually inspected all spectra and correlation functions (which sometimes led to accepting redshift estimates with low correlation strength) we are confident to have missed only very few, if any, redshift estimates as a result of template mismatch.

The positions of the peaks in the correlation function were found from fitting a parabola to the 5 points around the peak. For each peak, we determined the S/N-ratio (the R-parameter defined by Tonry and Davis), while the uncertainty in the redshift estimate was found from the noise in the correlation function and the curvature of the peak. As already mentioned, each spectrum was visually inspected, together with its correlation function. The reality of each redshift was then judged from the positions of the major absorption lines, indicated on the spectrum for the redshift corresponding to a particular peak in the cross-correlation spectrum.

In Fig. 2 we show the distribution of the 5070 absorption-line redshift estimates that were accepted (of which a few were later rejected, from a comparison with emission-line redshifts, see Sect. 4.3) with respect to the S/N-ratio of the correlation peak, and redshift. The non-uniform redshift distribution is the result of the superposition of more than 100 clusters. The detailed analysis of the galaxy redshift distributions in our survey will be the subject of a separate paper.

In a completely independent effort, all Optopus CCD-frames were inspected for the presence of emission lines. The advantage of inspecting the frames rather than the extracted spectra is that emission-lines have far 'softer' and 'rounder' images than cosmic-ray events, and can thus be distinguished much better from the latter in the frames than in the one-dimensional spectra. At this point, no information on the absorption-line redshift was used. I.e. the inspection of the spectra was not limited to those wavelength intervals where emission lines could be expected, or to those spectra for which an absorption-line redshift had been obtained. In the wavelength range covered by our observations, and for the redshifts of our clusters, the principal emission lines that are observable are OII (3727 Å), H-β (4860 Å) and the OIII (4959+5007 Å) doublet. Especially the combination of the latter two features facilitated the recognition of the lines. Finally, fits were made to the uncleaned, wavelength-calibrated spectra in order to determine the wavelengths of the suspected emission-lines, and the implied redshifts. From the comparison with the absorption-line redshifts (see Sect. 4.2) it is found that the estimated errors in the emission-line redshifts are between 40 km/s for redshifts based on more than one emission line, and 80 km/s for redshifts based on a single line.

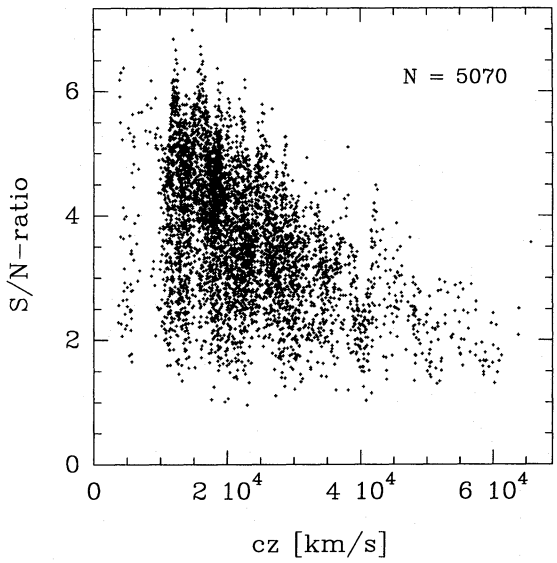

Fig. 2. The S/N-ratio of the peak in the cross-correlation function against redshift for the 5070 galaxies for which an absorption-line redshift was determined.

In total, the 175 Optopus exposures (with multiple exposures of a plate counted as one exposure) have yielded redshift estimates based on the absorption-line spectrum for 5070 galaxies, and redshift estimates based on emission lines for 1252 galaxies. For 360 galaxies, independent observations (on purpose!) have yielded more than one estimate of the absorption-line redshift, while for 47 galaxies at least two independent estimates of the emission-line redshift were obtained. For 666 galaxies, both an absorption- and an emission-line redshift were estimated independently. In total we have obtained for 5634 galaxies a redshift estimate, which corresponds to an average of more than 32 galaxy redshifts per exposure.

In considering this average number of galaxy redshifts per Optopus exposure, it should be noted that per exposure on average 1 of the candidate galaxies turned out to be a star, while one or two fibres per exposure were (purposely) positioned on blank sky. It is evident that for spectroscopy of objects with the average surface density of galaxies in rich clusters down to an integrated R-magnitude of about 17.5, the Optopus system with 50 fibres is ideally suited and very efficient.

4. The reliability and quality of the redshift estimates

As our spectroscopic data will be used for several types of analysis, either by itself or in combination with literature data, it is important that we assess the quality and reliability of our redshift estimates. We will discuss the following aspects of the reliability and quality of our data. First, we will show that our redshift estimates are not biased. Then we will discuss the reliability of individual redshift estimates, which we derive from the multiple, independent estimates within our dataset. These multiple measurements are also used to ascertain that the error estimates that we quote for the derived redshifts are indeed 1-sigma errors. Finally, we show that there is good agreement between our data and the literature data that is available for some of the clusters that we observed.

4.1. The redshift scale

Galaxy redshifts that are derived from cross-correlation of the spectrum with a template galaxy spectrum are, in principle, prone to biases which may result from imperfections in the wavelength calibration of the galaxy and/or template spectrum. For the spectra of the programme galaxies, we established the correctness of the linearity and zero-point of the wavelength scale to within 0.2 Å from lamp spectra and sky-lines. Possible errors in the wavelength calibration of the M 31 template spectrum that we used could also produce biases in our redshift estimates that are difficult to detect within our dataset.

However, we checked that possible non-linearity and zero-point errors in the wavelength scale of the M 31 template are negligible for all practical purposes. First, we constructed a synthetic template spectrum at a radial velocity of exactly 0 km/s. On a perfectly flat continuum we superposed the absorption features that produce most of the weight in the correlation analysis, viz. Ca-II, G-band, Mg-Ib. The absorption lines were represented by Gaussians with a dispersion of 1.4 Å at the appropriate positions and with the appropriate strengths. This synthetic template is considered superior to the M 31 template as regards the absence of wavelength calibration errors, even though the absorption profiles are not perfect as far as shape is concerned. However, the synthetic template is clearly inferior to that of the M 31 nucleus as regards the correlation strength for actual galaxy spectra, because all secondary absorption features, which do contribute to the correlation amplitude, are absent from the synthetic template.

Cross-correlation of the synthetic template with a spectrum of the K-giant star HD 185781 (obtained by one of us with the 2.5-m Isaac Newton Telescope at La Palma), yields a heliocentric radial velocity of -65 km/s for the latter. Although this does not agree very well with the value of -80 km/s given by Abt and Biggs (1972), it is in excellent agreement with a more recent determination by Mayor (priv. comm.), who found -67 ± 0.3 km/s. Having confirmed the correctness of the zero-point of the synthetic template, we then cross-correlated the synthetic template with the M 31 template. This yielded a heliocentric radial velocity of -306 km/s for M 31, which is very close to the value of -295 ± 7 km/s given by de Vaucouleurs et al. (1991). This again confirms the correctness of the zero-point of the synthetic spectrum, and shows that the wavelength scale of the template spectrum is also correct. This latter conclusion is also borne out by the data in Fig. 3. Here we display the difference between redshift estimates for 3065 of our programme galaxies, for which correlation with both the M 31 and the synthetic templates yielded redshift estimates with a S/N-ratio ≥ 3. On the basis of Fig. 3 we estimate that any remaining deviation of our redshift scale from the correct one amounts to less than 15 km/s per $\Delta z = 0.1$.

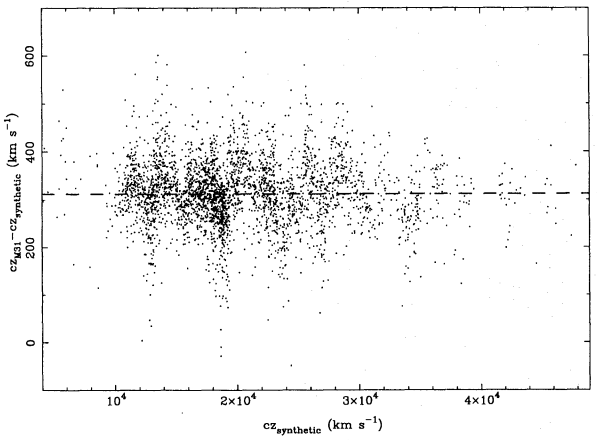

Fig. 3. The difference Δz between the redshifts obtained with the M 31 template and with the synthetic template, as a function of redshift. We show the 3065 galaxies for which the cross-correlations with the M 31 and the synthetic template both have a S/N-ratio ≥ 3. From these data we conclude that the non-linearity of our redshift scale is at most 15 km/s per $\Delta z = 0.1$. The dashed line corresponds to the velocity of the M 31 template

4.2. The reliability of the redshifts

There are two properties of a redshift estimate that are important. First there is the uncertainty of the estimate, or rather: its estimated error. Second, there is the reliability of the estimate, i.e. the probability that a second, independent measurement will produce the same result to within the limits set by the uncertainty of both estimates. For absorption-line redshifts, the uncertainty of the estimate follows from the curvature of the peak of the cross-correlation function, in combination with the noise in the correlation function. An empirical check of the correctness of the estimated errors is discussed below.

The reliability of an absorption-line redshift is equal to 1.0 minus the conditional probability that any of the peaks in the correlation function, other than the accepted peak, is the true indicator of the redshift of the galaxy. If the accepted peak is the highest one (which is very frequently, but not always, the case), it can be shown (see Tonry and Davis 1979) that the reliability of the derived redshift is (very) small when the amplitude of the correlation peak is low in comparison to the fluctuations in the correlation function. The ratio between the amplitude of the peak and the RMS value of the fluctuations is generally referred to as the S/N-ratio of the correlation peak. The reliability as a function of S/N-ratio approaches a Heaviside function, i.e. for high values of the S/N-ratio the reliability is very close to 1, while in a rather narrow range of S/N-ratio the reliability changes from essentially 0 to 1.

In the following, we have not attempted to derive from first principles the detailed dependence of the reliability on the S/N-ratio of the correlation peak. Instead, we use a schematic representation in which we assume that above a certain limiting S/N-ratio all reliabilities are equal to unity. Below this limit we subsequently are interested only in the average reliability of the available redshifts (which thus automatically involves the distribution of the S/N-ratios below the limiting value). In Appendix A we first use a set of two double exposures to derive a limiting S/N-ratio of 3.0 above which the reliability is unity. Below this value we find an average reliability of 0.6. It should be realized that this latter number applies only when, in each and every correlation function, the dominant peak is blindly accepted as the indicator of the redshift. As explained before, it is also valid *only* for the particular S/N-ratio distribution in the two double exposures.

The simultaneous visual inspection of the galaxy spectra, and their correlation functions (as discussed above) has yielded the verdict 'highly improbable' for quite a few redshift estimates with S/N-ratio < 3.0, and such estimates have been rejected. In Appendix A we derive an empirical estimate of the reliability of the redshift estimates in the sample of 5070 absorption-line redshifts that were *accepted* after visual inspection of the spectra and correlation functions. We confirm (from multiple measurements) that the average reliability of the estimates with S/N-ratio ≥ 3.0 is larger than 0.99. The average reliability of the *accepted* estimates with S/N-ratio < 3.0 turns out to be about 0.95.

The reliability of the emission-line redshifts has also been estimated empirically from double measurements. As described in Appendix A, it turns out that emission-line redshifts based on at least two lines have a reliability that is larger than 0.95. Redshifts based on only one emission line have an average reliability of about 0.8 (but the uncertainty in this number is of order 0.1).

Finally we have used the (dis-)agreement between absorption- and emission-line redshifts for the 666 galaxies for which we could determine both, to improve our reliability estimates. As detailed in Appendix A, we find reliabilities of 1.00 for S/N-ratio ≥ 3.0 absorption-line redshifts, of 0.95 for the accepted S/N-ratio < 3.0 absorption-line redshifts, of 0.97 for multiple-line emission-line redshifts and of 0.81 for single-line emission-line redshifts.

4.3. The construction of the redshift catalogue

With the reliabilities derived in the previous paragraph in mind, we have constructed our final redshift catalogues as follows.

First, we include all 4403 accepted galaxy redshifts based on *absorption lines only*, as well as the 565 galaxy redshifts based *only on one or more emission lines*. In the case of concordant multiple measurements we have adopted the estimate with the highest S/N-ratio (absorption lines), or from the largest number of (emission) lines.

Second, for the 666 galaxies with *both absorption- and emission-lines* we have determined the redshift as follows. For the 586 galaxies for which the two estimates agree to within 500 km/s (with the large majority of the differences less than about 200 km/s), the redshift is computed as the unweighted average of both estimates. In the 80 cases where the estimates disagree, we generally accepted the estimate in the category with the highest average reliability. This means that all 57 discordant single-line emission-line redshifts were ignored, as well as the

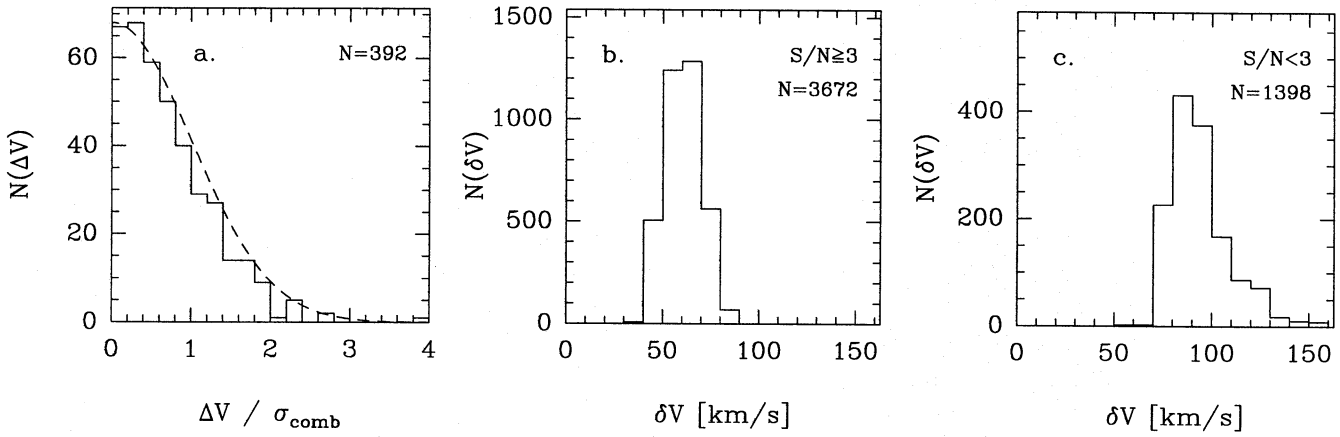

Fig. 4. a The distribution of the absolute value of the velocity difference (in units of the combined estimated errors) for 392 independent pairs of multiple absorption-line redshifts. A Gaussian with dispersion of unity and normalized to the total number of pairs is shown for comparison. **b** The distribution of the error estimates for the 3672 absorption-line redshifts with S/N $\geq$ 3. **c** The distribution of the error estimates for the 1398 absorption-line redshifts with S/N $<$ 3.

3 multiple-line emission-line redshifts that were not concordant with S/N-ratio $\geq$ 3.0 absorption-line redshifts. However, 18 of the 20 S/N-ratio $<$ 3.0 absorption-line redshifts that were not concordant with multiple-line emission-line redshifts were ignored, but 2 were accepted, because the emission-line redshift turned out to be unacceptably low. This produces a catalogue of 5634 galaxy redshifts with an estimated overall reliability of 0.98; i.e. we expect not more than about 120 redshifts in our catalogue to be erroneous.

4.4. The uncertainties in the redshift estimates

The formal uncertainty of an absorption-line redshift estimate follows directly from the curvature of the peak in the correlation function and the noise (Tonry and Davis 1979). We have empirically checked the statistical meaning of the error estimates using the multiple absorption-line redshift estimates with S/N-ratio $\geq$ 3.0 for 265 galaxies, which form 392 independent pairs. In Fig. 4*a* we show the distribution of the absolute value of the velocity difference for these 392 independent pairs expressed in units of the two error estimates added in quadrature. It can be seen that the distribution is indeed close to normal with a dispersion of unity, which confirms that the error estimates are indeed 1-sigma errors. In Fig. 4*b* the distribution of the error estimates for the 3672 redshifts with S/N $\geq$ 3.0 is given, and in Fig. 4*c* the same is given for the 1398 redshifts with S/N $<$ 3.0.

The errors in the emission-line redshifts have been estimated as follows. There are 47 pairs of twice-measured emission-line redshifts. Of these, 30 are based on more than one line. For these pairs the RMS value of the absolute velocity difference is only 57 km/s. There are 14 pairs having one estimate based on a single line and another based on at least two lines. Two of these pairs are discordant, but the RMS value of the absolute velocity difference of the 9 concordant pairs is 129 km/s (or 95 km/s if the largest difference of 297 km/s is ignored). Finally, all three pairs consisting of two single-line redshifts are concordant.

Table 2. Comparison between ENACS and literature redshifts, for galaxies with position differences of not more than 20″.

Cluster	# galaxies total	# galaxies $\lvert\Delta V\rvert < 500$	$\langle\Delta V\rangle$ km/s	$\sigma_{\Delta V}$ km/s	ref.
A0119	59	41	-176	152	1
A0151	34	28	-96	193	2
A0168	10	8	13	58	3,4
A0548	29	27	-57	90	5
A0754	29	23	25	103	5,6
A0957	21	19	27	159	7
A1069	6	5	13	117	7
A1809	25	25	38	108	8,9
A2052	22	22	-17	121	9
A2717	17	17	-105	95	10
A3112	15	13	-58	215	11
A3128	16	16	17	72	10
A3158	16	14	-48	215	12,13
A3558	36	32	15	99	14
A3667	64	51	69	155	15
total		341	-23	130	

References: 1. Fabricant et al. (1993); 2. Proust et al. (1992); 3. Zabludoff et al. (1993); 4. Faber & Dressler (1977); 5. Dressler & Shectman (1988); 6. Zabludoff et al. (1990); 7. Beers et al. 1991; 8. Hill & Oegerle (1993); 9. Malumuth et al. (1992); 10. Colless & Hewett (1987); 11. Materne & Hopp (1983); 12. Chincarini et al. (1981); 13. Lucey et al. (1983); 14. Teague et al. (1990); 15. Sodré et al. (1992)

Their average velocity difference is also 95 km/s. We conclude that redshifts based on more than one line on average have very small estimated errors of about 40 km/s and are thus comparable to our 'best' absorption-line redshifts. Single-line redshifts are probably a factor of two less accurate.

4.5. Comparison with redshifts from the literature

For 15 of the clusters observed by us (viz. A119, A151, A168, A548, A754, A957, A1069, A1809, A2052, A2717, A3112, A3128, A3158, A3528, A3558 and A3667), galaxy redshifts have been published by other authors. We have cross-identified the galaxies on the basis of positional and velocity agreement, requiring that the position difference be less than 20′ and the velocity difference less than 500 km/s. The results are summarized in Table 2. We conclude that the agreement between our redshifts and those in the literature is very good. We do not find systematic velocity offsets at a level which would prevent a useful combination between our data and those from the literature.

5. The calibration of the photographic photometry

Wide-field photographic imaging with Schmidt telescopes is currently the fastest and only practical way to cover large areas of sky, and the POSS and SERC surveys together provide coverage of all our clusters. All photometry for the galaxies in our programme is based on these surveys, and was obtained during the construction of the galaxy catalogues. In order to establish the zero-points of the photographic photometry we have obtained CCD photometry for about half of our clusters.

Galaxy photometry is notoriously difficult, because there is no such thing as *the* magnitude of a galaxy. Basically the problem is that one needs to define an aperture within which the integrated brightness of the galaxy is determined. Due to the large variations in the brightness profiles of galaxies (both in slope and in characteristic scale), any aperture one cares to define (be it metric or isophotal) has a different physical meaning for different galaxies. In short: it is impossible to derive from the brightness distribution one single number that can be used in the same manner for all galaxies, without at the same time giving a pictorial description of the individual galaxies. This basic problem is very much in evidence in the calibration of the photographic photometry.

5.1. The photographic photometry

During the construction of the cluster galaxy catalogues, several object parameters were obtained from the plate-scanning with the *Astroscan* measuring machine (see Sect. 2.2). We used a detection threshold above sky of between 5 and 7 times the noise in the sky background. For the photographic photometry, this threshold also served as a limiting isophote. For each galaxy, the photometric parameter $P_{\rm phot}$ was derived as the square root of the sum of the photographic densities above sky within the isophote defined by the detection threshold.

For the 103a-E emulsion of the red PSS survey, this threshold thus corresponds to an isophote (above sky) of about 40% of sky. This number is based on a noise in photographic density of 0.05 per 500 μm^2 (the effective size of a resolution element) and $\gamma \simeq 2$ (the slope of the characteristic curve of the emulsion). For the IIIa-J emulsion of the green SERC survey, with corresponding values of 0.04 and 3.5, the detection threshold corresponds to an isophote (above sky) of about 20% of sky. The nominal values of the sky brightness are about 20 and 22 mag/arcsec^2 for the 103a-E and IIIa-J emulsions respectively. Hence, the limiting isophotes of our photographic photometry would be expected to be of the order of 21.0 and 23.5 mag/arcsec^2 on the red and green plates respectively. However, actual sky brightnesses are likely to be higher than these nominal, minimum values, probably by as much as 1.0 mag. This assumption is consistent with the practical plate limits for the detection of stellar objects on these plates of about 20.5 and 22.5 mag respectively. The actual values of the limiting isophotes will vary somewhat between clusters, primarily because of differences in sky brightness between plates, which are of the order of 0.2 mag (Dalton et al. 1992).

5.2. The CCD photometry

In order to calibrate the photographic photometry, we have obtained CCD-images of subsets of the galaxies in about half of our clusters. We used the 1.54-m ('Danish') and 0.92-m ('Dutch') telescopes at La Silla. In Table 3, we give a summary of the dates of the observations, the telescopes and filters used, and the clusters for which we obtained data. The weather was not always cooperative, and some of the data obtained are not of photometric quality. There are 4 clusters with very large internal spreads (of between 0.50 and 0.80 mag) with respect to the average calibration relation discussed below. We have excluded these clusters from the calibration, on the reasonable assumption that the large internal dispersions are due to non-photometric conditions.

For all galaxies in the CCD-frames for which photographic photometry was available, an isophotal R-magnitude within the 25 mag/arcsec^2 R-isophote (R_{25}) was determined (see e.g. Le Fèvre et al. 1986). For the galaxies that had B-band CCD-data available as well, the B-band isophotal magnitude within the 25 mag/arcsec^2 B-isophote (B_{25}) as well as the B-R colour within the 25 mag/arcsec^2 R-isophote $(B-R)_{25}$ were also determined. One might argue that a much brighter isophote should have been chosen, in order to adhere more closely to the apertures in the photographic photometry. That would certainly have decreased the influence of the shapes of the individual galaxy brightness profiles on the photometric calibration, although it would be very difficult to achieve identical apertures for all objects in the two sets of photometry. By adopting R_{25} we have wilfully accepted a larger influence of the variety of the shapes of galaxy brightness profiles in our calibration, but we have ensured uniformity and compatibility with many programs of galaxy photometry in the literature.

5.3. The quality of the calibration

In Fig. 5 we show the relations between the photographic magnitude, i.e. $P_{\rm phot}$, and the isophotal R-magnitude (R_{25}) derived from the CCD-imaging, for 100 galaxies in 11 clusters scanned on PSS plates (red) and for 314 galaxies in 28 clusters scanned on SERC IIIa-J plates (green). For R_{25} between about 14 and 18, the relation between the logarithm of $P_{\rm phot}$ and R_{25} appears

Table 3. Some details of the CCD photometry.

Observing period		Tel.	Filters	Clusters
01/11 – 06/11	1989	1.54-m	B,R	A2717, A3009, A3108, A3141, A3158, A3223, A3795, A3822
25/04 – 28/04	1990	1.54-m	B,R	A0754, A0957, A0978, A1069, A1399, A1809, A2029, A2040, A2048, A3528, A3558, A3559, A3562
17/10 – 18/10	1990	1.54-m	B,R	A0151, A2426, A3094, A3667, A3864
08/10 – 10/10	1991	0.92-m	R	A0168, A0367, A2383, A2480, A2764, A2819, A2915, A3112, A3122, A3264, A3651, A3691, A3799, A3809
24/11 – 29/11	1992	0.92-m	R	A0295, A0514, A0548, A2734, A3128, A3142, A3341, A3825

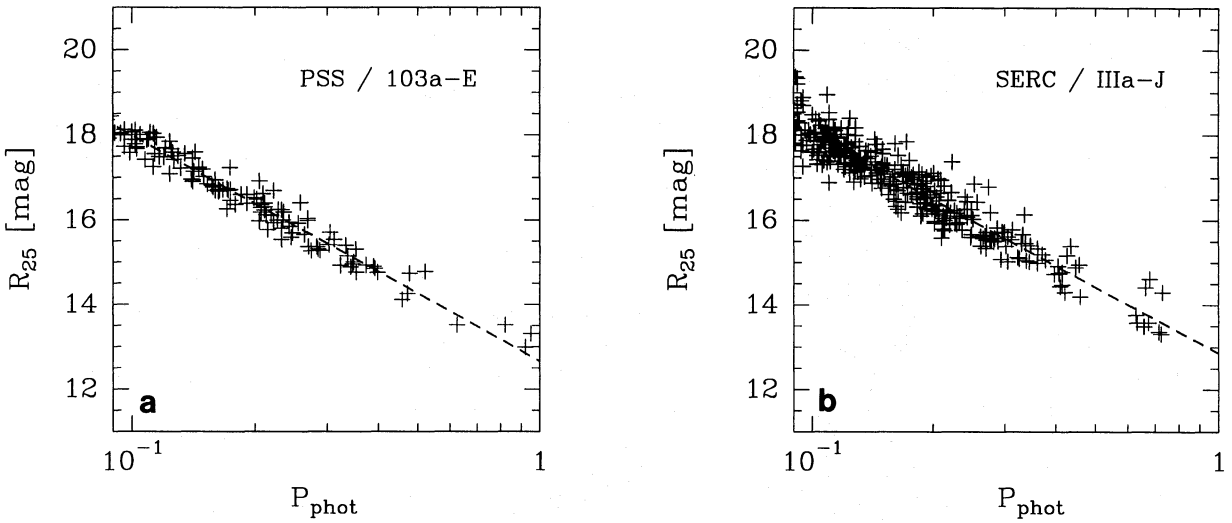

Fig. 5a and b. The calibration relations between the photometric parameter $P_{\rm phot}$ and the R_{25} isophotal CCD magnitude for (**a**) the 103a-E emulsion of the red PSS survey and (**b**) the IIIa-J emulsion of the green SERC survey. Note that the individual zero-points of the clusters have been taken into account.

indeed to be quite linear, with a slope not very different from 5.0 (the zero-order expectation). In producing the calibration relations in Fig. 5, we have taken out differences in the zero-points for individual clusters, which are to be expected as a result of the variations in limiting isophote. As fits to the individual calibration relations do not reveal significant differences in slope, we determined the zero-points from a maximum-likelihood fit to the calibration data that solves simultaneously for a universal slope and individual zeropoints per cluster. The global dispersions with respect to the average relations in Fig. 5 are 0.24 and 0.34 mag for the PSS and SERC calibrations respectively.

The dispersion in the global calibration relations consists of the following contributions. First, there are random measuring errors in the photometry. Second, there is a contribution due to the differences in limiting isophotes, which makes itself felt through the large variation in brightness profiles of galaxies. As a result, the correlation between the two isophotal magnitudes is far from perfect. In a calibration dataset like ours one thus expects a systematic dependence of the difference between the two magnitude estimates on the ratio of the isophotal apertures, as that ratio reflects the 'slope' of the brightness distribution. Finally, there is an extra contribution to the spread in the SERC calibration relation from the appreciable range in galaxy colours, which is a result of the fact that we compare red CCD magnitudes to green photographic magnitudes.

Both the aperture and the colour effect are clearly detectable in our calibration data. The aperture effect is, to first order, proportional to the logarithm of the ratio of the two apertures, $\log(A_{\rm CCD}/A_{\rm phot})$. The global slope of the calibration relation, the individual zero-points of the clusters and the coefficient of the aperture ratio were all obtained from a combined maximum-likelihood fit to the relation between R_{25} and $P_{\rm phot}$ for all galaxies in the sets of clusters that were scanned on the same emulsion. We find that the size of the aperture effect is about 0.5 mag per decade in aperture ratio for the PSS data and about 1.0 mag per decade for the SERC data. The factor of two difference between the two constants is due to the difference in contrast index of the two emulsions. The colour effect was found, from a limited subset of clusters with $(B-R)$-data, to amount to about 40% of the measured $(B-R)_{25}$ colour. This seems reasonable since the SERC IIIa-J passband is quite a bit redder than B, while for red galaxies the effective wavelength is even redder than average.

Table 4. Zero-points and internal dispersions of the photometry for clusters with useful calibration data.

Cluster	Δ zero	σ_{mag}	N_{gal}	colour
A0151	0.04	0.28	15	R
A0168	-0.03	0.14	3	R
A0295	-0.14	0.16	8	R
A0367	-0.17	0.15	16	G
A0514	-0.05	0.37	25	G
A0754	-0.52	0.20	13	R
A0957	-0.14	0.16	8	R
A0978	0.06	0.18	8	R
A1069	0.40	0.20	11	R
A1809	0.14	0.36	9	R
A2040	-0.02	0.32	13	R
A2048	0.03	0.28	16	R
A2383	-0.21	0.47	10	G
A2426	0.20	0.35	4	R
A2480	-0.15	0.15	4	G
A2717	-0.27	0.49	6	G
A2734	0.56	0.32	5	G
A2764	0.05	0.35	7	G
A2819	-0.09	0.30	38	G
A2915	0.28	0.49	6	G
A3009	0.45	0.40	4	G
A3094	0.51	0.33	5	G
A3108	0.30	0.41	6	G
A3112	-0.23	0.38	13	G
A3122	0.29	0.34	10	G
A3128	-0.12	0.34	28	G
A3141	-0.29	0.29	3	G
A3142	0.42	0.40	6	G
A3158	-0.12	0.25	14	G
A3223	0.13	0.40	14	G
A3264	0.20	0.45	11	G
A3528	-0.51	0.22	16	G
A3558+59+62	1.69	0.44	13	G
A3651	-0.26	0.41	10	G
A3667	-0.39	0.48	27	G
A3691	-0.16	0.31	14	G
A3795	-0.18		2	G
A3809	0.03	0.47	6	G
A3822	-0.01	0.35	4	G
A3864	-0.02	0.30	4	G

For the subset of galaxies for which we have information on the aperture-ratio and on the $(B-R)$ colour we find that, when we correct for these effects by reducing all R_{25} values to a reference aperture-ratio and, where possible, to a reference $(B-R)$ colour, the global dispersion in the calibration relation indeed decreases, to a value of about 0.20 mag. This still includes a contribution from the variation in the 'slope' of the brightness distributions, and is thus consistent with estimates of the combined random noise in the photometry of about 0.15 mag.

Table 5. Comparison between ENACS and literature magnitudes, for galaxies whose positions agree to within 20″.

Cluster	# gal.	band	⟨Δmag⟩	$\sigma_{\Delta mag}$	ref.
A0119	59	R	0.39	0.10	1
A0754	33	R	-0.26	0.08	2
A2717	17	B_J	-0.98	0.11	3
A3128	16	B_J	-1.67	0.11	3
A3667	91	B_{25}	-1.70	0.22	4

References: 1. Fabricant et al. (1993); 2. Fabricant et al. (1986); 3. Colless (1989); 4. Sodré et al. (1992)

For the large majority of the galaxies for which we obtained redshifts we have no information on aperture-ratio or colour. To convert photographic magnitudes into R_{25}'s, we can thus do no better than apply the average calibration relations shown in Fig. 5 for these galaxies. For the 39 clusters for which we do have usable calibration data, and for which we could therefore estimate an individual zero-point, we applied the latter, even if it did not differ significantly from the average value. In Table 4 we show the values of the zero-point offset (individual cluster value minus average) as well as the internal dispersion for each of these 39 clusters. The Table gives an indication of the maximum zero-point errors that we are likely to have made for the clusters without calibration data.

When using our calibrated R-band photometry, the following points must be realized. First, within a cluster for which no individual zero-point is available, the relative photometry is not affected. In other words: for such clusters one can still study the luminosity distribution. However, when combining photometric data from several clusters, one has to know whether the zero-point of the photometry was estimated for the given cluster, or whether it was assumed to be equal to the average value. From Table 4 we estimate that the RMS value of the difference between the assumed and the actual zero-point for a cluster without individual calibration is 0.27 mag. For the clusters with calibration, one finds from Table 4 that the quality of the individual zero-points is of the order of 0.05 to 0.1 mag.

5.4. Comparison with photometry from the literature

For 8 clusters in our sample there are also magnitudes available in the literature. In 3 cases, viz. A0151, A0548 and A2052, the magnitudes were estimated by eye, and we did not use those data to check the quality of our photometry. For the remaining 5 clusters we show, in Table 5, the results of a comparison between our photometry and that from the literature. It must be realized that for A0754, A2717, A3128 and A3667 the literature data also consist of photographic photometry calibrated by CCD-imaging. For A119, the photometry is based on CCD-imaging of individual galaxies, at least for the brighter galaxies that carry essentially all of the weight in the comparison. Galaxies were cross-identified on the basis of positional agreement only; we required that the positional difference be less than 20″. From

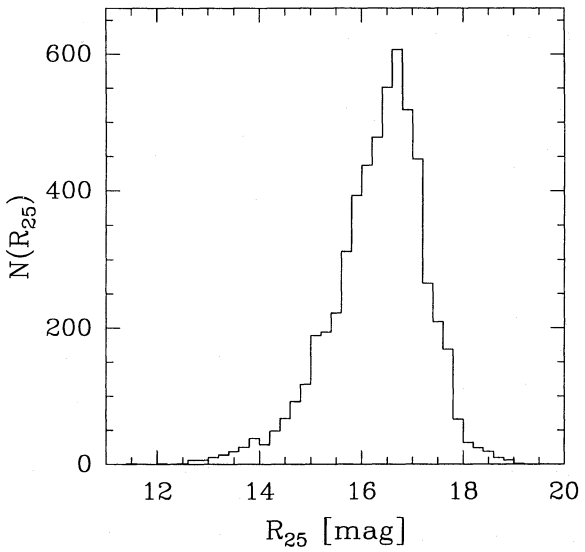

Fig. 6. The distribution of the R_{25} magnitudes of all 5615 galaxies.

Table 5 we conclude that the offsets Δmag between our data and the literature data are consistent with a spread of about 0.3 mag in the zero-points of our magnitudes.

The agreement with the photometry from the literature (as judged from the dispersion in Δmag) is better than one would expect from the dispersions $\sigma_{\rm mag}$ in our calibration relations, or from those reported by the other authors, for A119, A754, A2717 and A3128. This is not surprising because in those four cases we compare our photographic magnitudes directly to photographic magnitudes based on the same plate material. The dispersion in Δmag is then primarily due to the (unknown) differences in threshold in the two sets of photographic photometry (i.e. the aperture effect), and to the colour differences between galaxies. The larger dispersion in Δmag for A3667 is most likely due to the fact that the photographic magnitudes were converted from B_J to the isophotal B_{25} system, which probably introduces an additional aperture term.

5.5. The completeness of the redshift surveys

In Fig. 6 we show the combined apparent magnitude distribution for all 5615 galaxies for which we obtained a redshift (for technical reasons photographic photometry is lacking for 19 galaxies).

As explained in Sect. 2.2, we have attempted to measure a redshift for each of the 50 brightest galaxies in the region of each Optopus plate. That means that we obtained spectra for essentially all galaxies above a given limiting R_{25} magnitude, which for the different clusters varies between 17 and 18. However, not all spectra have yielded a redshift. There are several reasons for that, the most important ones of which are the following. First, an isophotal magnitude brighter than a given limit does not always guarantee a sufficiently bright central surface brightness. This seems to be true in particular for the brightest galaxies, which are quite large compared to the size of the fibres. As a result, a redshift was obtained on average only for 2.2 of the brightest 5 galaxies (and for 2.5 of the 5 next brightest galaxies). Variations between galaxies in the strengths of the absorption and emission lines also contribute to a less-than-100% score. At the faint end, i.e. near the magnitude limit this seems to be the main reason for lack of success.

We have calculated the completeness (i.e. the ratio of the number of redshifts obtained over the number of galaxies observed) for each cluster as a function of magnitude. The completeness increases in general from the brightest to intermediate magnitudes and then either stays constant or decreases somewhat towards the magnitude limit. Most clusters have a 'maximum' completeness at $R_{25} = 17.1 \pm 0.3$. For 52 clusters this maximum completeness is between 0.7 and 0.9. For 30 clusters it is between 0.6 and 0.7, and for the remaining 25 clusters it is below 0.6. Among these 25 are the 5 clusters that were already noted in Sect. 3.1 to have been observed in very bad conditions. Frequently, several redshifts are available beyond the magnitude at which the completeness is maximum, and therefore the maximally complete samples contain in total about 500 galaxies less than the 5634 for which we have measured redshifts.

Because the information on the completeness is relevant for some types of analysis, we will give details about it when we make available the full catalogues.

6. The identification of systems in redshift space

As we are interested in studying the properties of rich clusters of galaxies, our first concern is to define the physically relevant systems in our redshift surveys by identifying superimposed fore- and background galaxies. This problem is illustrated in Fig. 7, in which we present for each of our 107 target ACO clusters (lines of sight hereafter) the radial velocities in a 'barplot'.

Several methods have been proposed in the literature for identifying systems in redshift surveys in a more or less objective manner. In all existing methods some assumptions have to be made about the systems that one wants to detect, or some parameter has to be chosen which influences in a fundamental way the detection of systems or their properties. Because, as far as we know, there does not exist a method that is free from interpretation, we try to use a method that does not produce results that are clearly in conflict with either the qualitative visual impression from Fig. 7 or with well-established properties of clusters.

In the context of the present discussion we are only interested in defining the overall properties of the systems, i.e. their existence, their average redshift, and their approximate extent in velocity space. Therefore, a good method should on the one hand be able to separate the obvious physical systems from fore- and background galaxies. In addition it should separate systems if there is more than one in a pencil-beam survey. Finally, it should not break up physical systems into subsystems.

For many of the larger systems, consisting of several tens of galaxies, the overall properties will depend only weakly on the details of the method used. The main reason for this is that

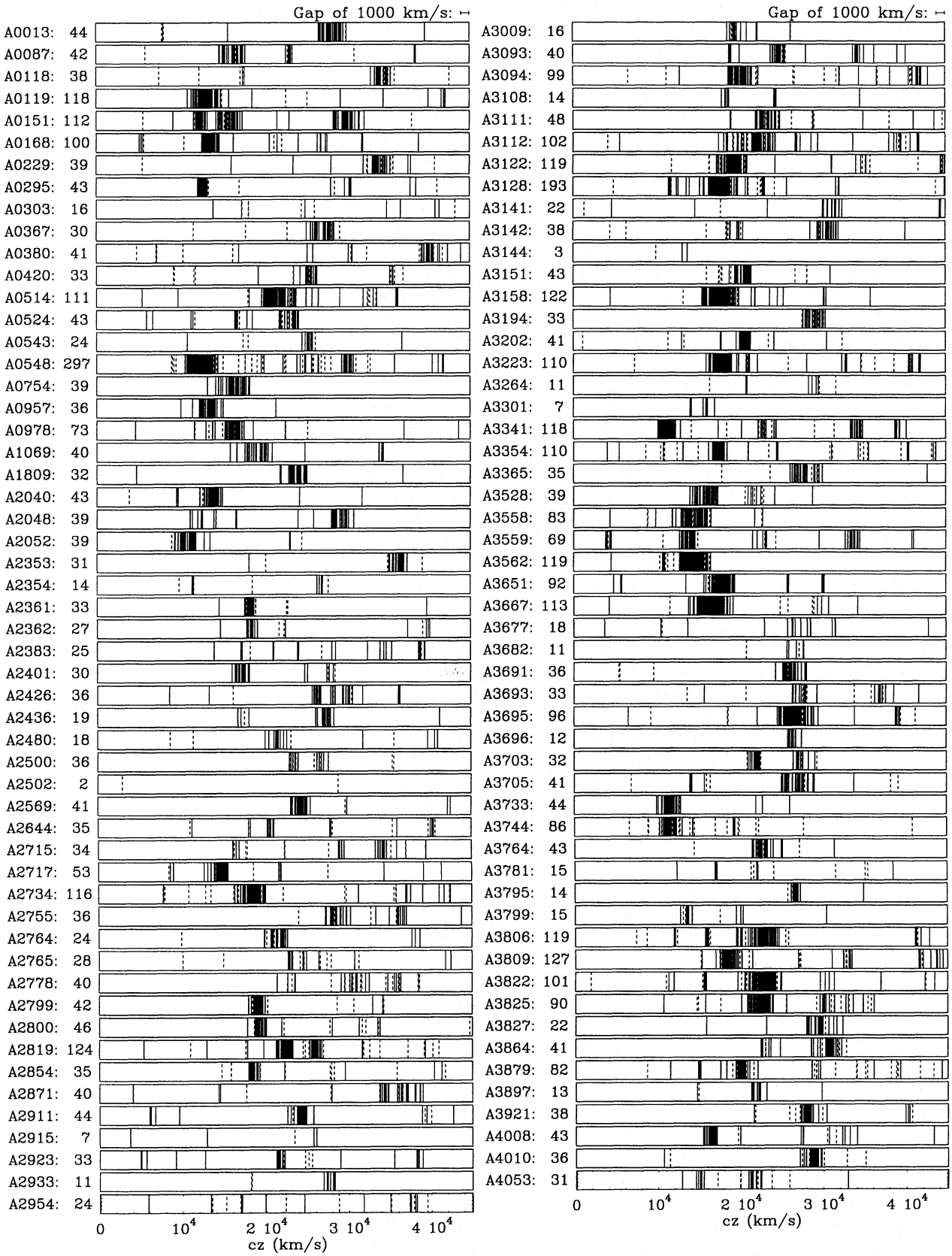

Fig. 7. Distribution of radial velocities in the directions of the 107 target ACO clusters studied in the ESO Nearby Abell Cluster Survey (ENACS). Solid bars indicate velocities derived solely from absorption lines, dashed bars indicate velocities derived from emission lines or from emission and absorption lines. The total number of galaxy redshifts in a survey is shown next to the Abell number of the cluster.

discretization is not important for such systems. However, it is probably unavoidable that the properties of the smallest system that the eye detects in Fig. 7 will depend rather strongly on the details of the employed method.

The velocity bar-plots in Fig. 7 show that the density contrast between the systems and the fore- and background galaxies is rather sharp. This quite naturally leads to two types of solution to the problem of system definition; one that uses the high density and compactness of the systems, and one that is based on the emptiness, the 'gaps' in velocity, between the systems. In the latter case, if two adjacent galaxies in the velocity distribution are to belong to the same group, their velocity difference should not exceed a certain value, the *velocity gap*.

An example of the first type of solution is the method proposed by Pisani (1993). In this method a cluster is defined as a single peak in the probability density that underlies the distribution of galaxies along the line of sight. The method is non-parametric, as it does not require an input parameter, such as a limiting gapsize. However, the method employs a limiting probability for assigning individual galaxies to a given system, which influences the properties of the resulting systems. As White (1991) illustrates with N-body models, clusters that are spatially compact do not necessarily show a single peak in velocity space. Therefore, the basic assumption of the method is probably not true for at least some of the systems. We have applied the method to our data with the probability limit proposed by Pisani, and found that it breaks up systems which we consider compact into smaller sub-systems. As we do not want to prejudice the separation of systems into possible sub-systems at this stage, we have decided not to use this method.

For a given physical system the distribution of gap sizes evidently depends on the number of velocities sampled, and on the velocity width of the system. To ensure uniformity in the definition of systems, the limiting gapsize should therefore, at least in principle, take into account the number of velocities measured for a given system as well as the velocity dispersion. However, because these are exactly the properties we are trying to define for a given system, the limiting gapsize must be estimated from the velocity width and population of the well-sampled systems, of which the global definition is not problematic.

Zabludoff et al. (ZHG 1990) propose a two-step scheme along these lines, in which first a fixed gap of 2000 km/s is applied to identify the main systems. Subsequently, a gap equal to the velocity dispersion σ_V of the system is applied, to eliminate outlying galaxies. In this case, the gap of 2000 km/s is based on the overall velocity widths of known clusters, while the second step employs the detailed information in the system that one is defining. We have used this method on our data, but find that we need to use a different choice of the parameters, in order to avoid the merging of separate systems into larger units (as happens e.g. in the case of A0151 and A2819). Because the ZHG method has been applied to find systems in a comparable survey in the north, we will discuss it in some more detail below.

Another possible method considers gaps as the result of a Poissonian process, with the expectation value of the gapsize chosen equal to the median gapsize. The motivation for this method is again that it does not require a physical input parameter, only the specification of a limiting probability. Large gaps with a probability smaller than the specified limit define the physical systems. The method works well for the well-sampled surveys and the results then do not depend critically on the choice of the limiting probability. However, for lines of sight with less than about 30 redshifts, most gapsizes are close to the median value and the method is no longer sufficiently discriminative.

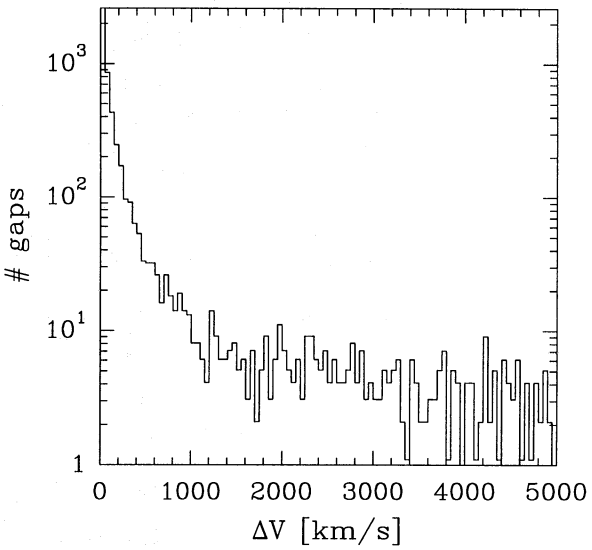

Fig. 8. The distribution of the velocity differences between galaxies (within a survey) that are adjacent in redshift, summed over all 107 surveys.

Ideally, we want to use the information contained in our redshift surveys, about the well-sampled as well as the less well-sampled systems. We also want to avoid making assumptions about e.g. the velocity dispersions of the systems in our surveys. Therefore, we have determined for each survey the distribution of the velocity gaps between galaxies adjacent in redshift, and summed these 107 distributions. The result is shown in Fig. 8. It is clear that for small gaps the distribution is determined by the internal velocity structure of the real cluster systems. The very large gaps, which occur between galaxies that are not associated with the systems, are more or less uniformly distributed. The optimal choice for the definition of systems is therefore the smallest gap value for which the distribution in Fig. 8 is still flat. For such a gap, galaxies that are associated with the systems are not separated, while most of the field galaxies will not be linked to the systems. On the basis of the distribution in Fig. 8, we adopt a value of 1000 km/s for the definition of the physically relevant systems in our survey.

In Table 6 (at the end of this paper) we list the properties of the 220 systems with at least 4 members, identified using a 1000 km/s fixed gap, in the 107 lines of sight observed in our ESO Nearby Abell Cluster Survey. The choice of the lower limit of 4 members is motivated by a comparison between the systems defined with a fixed gap of 1000 km/s and those defined with

the method proposed by ZHG. With the latter method all main systems in Table 6 are also found, with essentially the same average redshifts, except for the two systems with a velocity difference of about 4000 km/s in A151 and the two systems in A2819 with a similar velocity difference. The system definition according to ZHG merges both sets of systems which, on the basis of the redshift histograms, we do not consider acceptable.

For the smaller systems, in particular those with N$\lesssim$10, the merging of separate groups in our list into single systems by the ZHG method is a fairly common phenomenon. In some cases, the elimination of outlying galaxies on the basis of the provisional value of the velocity dispersion breaks up systems (defined with our method) in two sub-systems, while in a few other cases our method does not define a (small) system while the ZHG method does. In general, these effects confirm that the definition of small systems (say, with $\leq$ 10 members) is influenced by noise and by the details of the method. Most of the N<4 systems that are defined with our method are not found by the ZHG method. In Table 6 we have indicated on which N$\geq$4 systems our fixed-gap method and the ZHG method disagree.

Note that no systems were found in the direction of the cluster candidates A2502 and A3144; however, both were observed in very poor conditions. Note also that we have not listed velocity dispersions. This is because the system definitions in Table 6 are based only on the redshift distributions. Because it is not certain at this stage that each and every galaxy within the redshift limits of a system is indeed a member of that system, one must discuss the plausibility of the membership of each galaxy on the basis of velocity *and* position information, to obtain a dynamically meaningful estimate of the global velocity dispersion (see e.g. den Hartog and Katgert 1995 and Mazure et al. 1995). We refer to the latter for a determination of the distribution of global velocity dispersions, based on the data presented here in combination with data from the literature.

7. Field contamination and superposition effects

Abell (1958) and Abell et al. (1989) identified clusters, from visual inspection of survey plates, as overdensities in a 2-dimensional projection of a 3-dimensional galaxy distribution. It is evident from Fig. 7 that a very large fraction of the rich and nearby Abell cluster candidates that we studied are coherent structures in velocity space. However, at the same time, the bar-plots also clearly show the importance of superposition effects, which certainly will have influenced to some extent the observed 2-dimensional characteristics of clusters, such as richness or morphology.

The amount of field contamination in our survey can be quantified as follows. About 75% of the 5634 galaxies are in the largest system found in the direction of each of the rich Abell cluster candidates. Note that this number refers to the galaxies within $\approx 1\ h^{-1}$ Mpc of the cluster centre and down to $R \approx 17$, and that it applies to clusters with $z \lesssim 0.1$. Field contamination is thus found to be quite substantial for such clusters. However, about half of the 1422 galaxies that are outside the main systems are not in the field either, but in a secondary system. Field contamination in the strict sense of the word therefore probably amounts to at most 12% in our survey.

From the data in Table 6 we have calculated the fraction of redshifts in each pencil beam that is contained in the main system. In 85 out of 103 cases (we ignored the 4 pencil beams with less than 10 measured redshifts), i.e. in 83% of the cases, the main system is found to contain at least half of the total number of measured redshifts. It is of interest to compare this with an earlier estimate by Lucey (1983). Using models of the galaxy distribution, Lucey concluded that between 15 and 25 per cent of the clusters in the Abell catalogue have a true galaxy population that is less than half the apparent population of the cluster. Although our result and Lucey's estimate refer to slightly different apertures and to different redshift ranges, the agreement is quite satisfactory. In our data there is a clear dependence of this fraction on the total number of measured redshifts in the pencil beam. Of the 31 pencil beams with at least 46 measured redshifts, 29 (i.e. 94%) have a main system with at least half of the total number of redshifts; on the contrary: of the 35 pencil beams with less than 35 redshifts, 24 (i.e. 69%) have a main system with at least half the total number of redshifts. As the number of redshifts that we obtained correlates more or less with richness, this trend is not unexpected.

Field contamination will thus have influenced the richness of some of the clusters appreciably. Any cluster sample complete with respect to apparent richness will contain some clusters that should not be in the sample (those with higher-than-average contamination), while some clusters that should be in the sample will not have been included as a result of lower-than-average contamination. However, Lucey (ibid.) finds that contamination modifies the richness distribution of a cluster sample only slightly. In our discussion of the distribution of velocity dispersions for a complete, volume-limited cluster sample (Mazure et al. 1995) we study the effect of field contamination on richness, and in particular its effect near the richness limit of the sample.

A related question concerns the number of spurious rich clusters that result from the superposition of two poorer systems. As there is no unique definition of a spurious cluster, we will consider an Abell cluster candidate to be spurious if at least two redshift systems are found, with the number of redshifts in the main system exceeding that in the next richest system by not more than a factor of two. We have estimated the fraction of such spurious clusters in our sample as follows. In 18 out of 103 cases we find a secondary system with at least half as many galaxies as in the main system. However, this is very likely to be an overestimate of the true fraction of spurious clusters, for the following reason. The large majority (13 out of 18) of these cases occur when the number of redshifts in the secondary system is less than about 10. It is thus likely that small number statistics has artificially raised the number of spurious clusters. If we limit ourselves to the 64 cases in which the total number of redshifts in the main and (if present) secondary system is at least 30, we find that only 5 (i.e. 8%) of our clusters are spurious according to the above definition. If, alternatively, we base our estimate on the 79 cases in which the number of redshifts in the

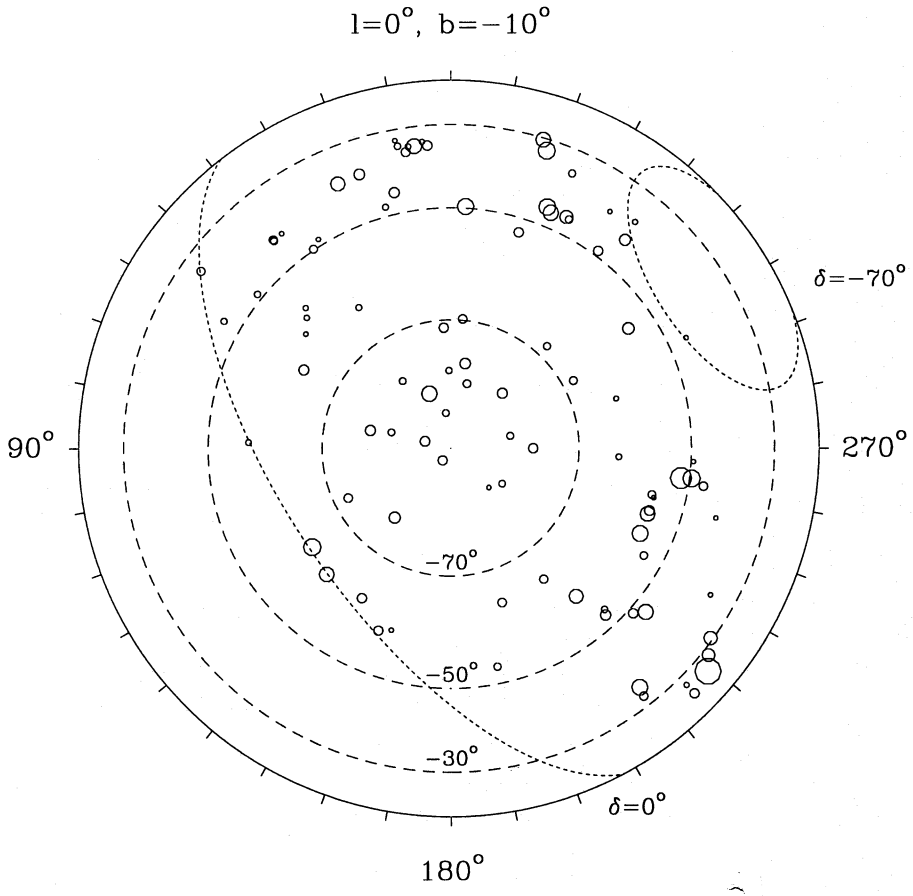

Fig. 9. The distribution on the sky of the 96 lines of sight in ENACS that have $b \leq -10°$. Dashed lines are at constant values of galactic latitude, the two dotted lines are at constant declination. The symbols indicate the lines of sight and their size reflects the number of galaxies found in the main system in the corresponding redshift survey.

main system exceeds 15, we find that 10 % of the clusters is spurious.

Although it is thus not completely straightforward to make a statement about the number of spurious clusters in our sample, we conclude that probably only in about 10% of the cases an $R \geq 1$, $z \leq 0.1$ entry in the ACO catalogue is the result of a superposition of two almost equally rich (but relatively poor) systems. This would imply that 8 of the 10 apparently spurious clusters among the 24 clusters with ≤ 15 redshifts in the main system must be attributed to small number statistics, which does not seem unreasonable.

Our conclusion that about 90% of the rich and relatively nearby ACO cluster candidates that we studied appear to be real rich clusters might, at first sight, seem to be in conflict with the result of Sutherland (1988). From a comparison of the angular and radial correlation functions of Abell clusters, Sutherland concluded that superposition must play an important rôle. However, it must be realized that his analysis was based on a sample which included many clusters of richness 0, for which superposition presumably is much more serious than for our $R \geq 1, z \leq 0.1$ clusters. Therefore, we do not consider the result of Sutherland to be in conflict with our data.

8. The spatial distribution of clusters and galaxies

In Fig. 9 we show the distribution on the sky of the 96 pencil-beam surveys for which $b \leq -10°$. The size of the symbols reflects the number of galaxies found in each of the main systems found in these surveys. The dotted lines indicate the declination limits of the ENACS. In a companion paper (Mazure et al. 1995) we will discuss the completeness of the set of clusters that one obtains by combining the main systems in Fig. 9 with data from the literature.

There are a few remarkable concentrations of clusters to be seen in Fig. 9. Some of these are probably due to chance superposition but a few correspond to well-known superclusters. The concentration in the region $245° \leq l \leq 265°$, $b \approx -54°$ is part of the Horologium-Reticulum supercluster (Lucey et al. 1983), and contains A3093, A3108, A3112, A3122, A3128, A3158, and possibly A3202. Three other concentrations, viz. those at $l \approx 230°$, $b \approx -25°$ (containing A548 and A3341), at $l \approx 7°$, $b \approx -35°$ (containing A3682, A3691, A3693, A3695, A3696 and A3705), and at $l \approx 338°$, $b \approx -46°$ (containing A3806, A3822 and A3825) were already detected by Zucca et al. (1993), on the basis of more limited redshift information.

In Fig. 10 we show for the 28 ('structure') clusters, for which several Optopus fields were defined, the projected distribution of the galaxies for which we obtained redshifts. The size of the symbols indicates the apparent brightness of the galaxies, while the outer contours delineate the outer boundary of the area covered by the Optopus plates. It is clear from this Figure that the coverage of the cluster galaxy distributions by several relatively small (33′) aperture plates introduces a special selection filter.

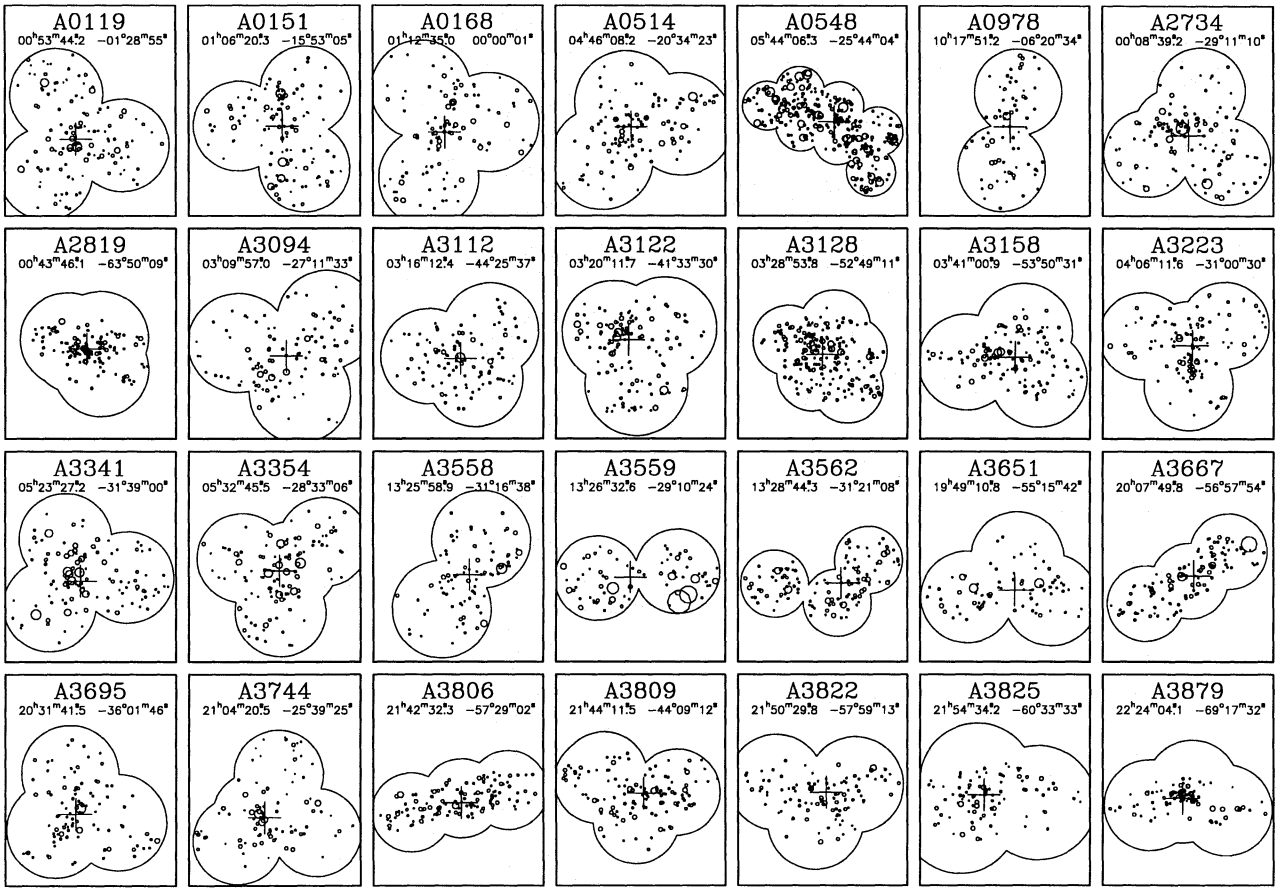

Fig. 10. The projected distribution of galaxies with a measured redshift, in the 28 'structure' clusters for which more than one Optopus aperture plate was used. The size of the symbols is an indication of the brightness of the galaxies. The median position of the galaxies is indicated by a cross, and listed as well. The diameter of the Optopus plates is 33′.

For each cluster the plates were positioned to optimize both the number of measured redshifts (where possible taking into account the availability of redshifts in the literature) as well as the area covered. In most cases the positioning of the plates simply reflects the distribution of galaxies in the cluster. The selection functions displayed in Fig. 10 are, to some extent, arbitrary and reflect our choice to try and measure as many bright galaxies in a large, not necessarily circular area, rather than going to fainter magnitudes in a smaller, circular area. For several applications the spatial filter does not affect the analysis. If it does play a rôle, e.g. when the total luminosity inside a projected distance from the centre or the uniformity of the magnitude limit becomes important, the spatial filters are known in sufficient detail that they can be taken into account.

9. Discussion and conclusions

Even without a detailed analysis of the properties of the systems that we identified, a few conclusions can already be drawn from the information in Table 6 and the data displayed in Fig. 7.

First, it appears that the large majority of the $R \geq 1$ ACO clusters with $z \leq 0.1$ (or with $m_{10} > 16.9$) that we observed indeed correspond to physical systems that are compact in redshift. Second, the effects of superposition are not negligible, but should at the same time not be exaggerated. Even for the clusters with only a relatively small number of redshifts available, most of the redshifts are generally contained within the dominant system. In other words: it does not happen very often that an apparently rich cluster in the ACO catalogue turns out to be the result of a superpositon of two, about equally rich systems. Only A151 (for which this was already known) and A2819 are good examples of this kind of superposition among the clusters with a large number of measured redshifts. In the class of the clusters with a more modest number of available redshifts A2426, A2500, A2778, A2871, A3108 and A3703 may be cases of clusters of which the apparent richness has probably been boosted significantly as a result of the superposition of two about equally rich systems. In quite a few of these cases, the velocity difference between the two systems is not larger than 3000 to 4000 km/s.

The summary of our programme in Figures 7, 9 and 10 immediately suggests several questions that one can ask from these data, either in isolation or in combination with data in the literature; and we are presently pursueing several of these. First, and

Table 6. Properties of the 220 systems with N≥4 found in the 107 lines of sight towards the ACO clusters in the ENACS.

ACO	N_z	z_{min}	z_{max}	$\langle z \rangle$	Literature		
					N_z	$\langle z \rangle$	ref.
A0013	4	0.026	0.027	0.027			
	37	0.089	0.100	0.094			
A0087	27	0.049	0.060	0.055			
	8	0.076	0.079	0.077			
A0118	4	0.058	0.059	0.059			
	30	0.110	0.120	0.115			
A0119	104	0.037	0.053	0.044	73	0.045	1
	4	0.139	0.140	0.140			
A0151	25^{m1}	0.039	0.044	0.041	8	0.041	2
	46^{m2}	0.048	0.058	0.053	37	0.054	2
	35	0.095	0.107	0.100	10	0.110	2
A0168	4	0.017	0.019	0.018	22	0.018	3
	76	0.042	0.049	0.045	28	0.045	3
	4	0.069	0.074	0.072			
	7	0.089	0.092	0.090			
A0229	32	0.107	0.119	0.113			
A0295	30	0.041	0.045	0.043	28	0.042	3
	5	0.100	0.102	0.102			
A0303	4	0.058	0.061	0.059			
A0367	27^{b3}	0.084	0.098	0.091		0.088	4
A0380	4	0.101	0.103	0.102			
	25	0.130	0.141	0.134		0.135	4
A0420	19	0.079	0.088	0.086			
	6	0.118	0.120	0.119			
A0514	90	0.066	0.080	0.072	2	0.073	5
	4*	0.084	0.089	0.085			
	8	0.107	0.112	0.110			
A0524	10	0.055	0.062	0.056			
	26	0.073	0.081	0.078			
A0543	10	0.082	0.088	0.085			
	9	0.166	0.176	0.171			
A0548	4*	0.030	0.032	0.031			
	237	0.035	0.051	0.042	133	0.041	5
	9	0.057	0.067	0.063			
	14^{m1}	0.080	0.094	0.087			
	21^{m2}	0.098	0.104	0.101			
	4	0.135	0.139	0.138			
A0754	39	0.044	0.061	0.055	86	0.053	5
A0957	34	0.038	0.051	0.045	36	0.045	3
					23	0.044	6
A0978	63	0.044	0.059	0.054	2	0.053	5
A1069	35	0.053	0.070	0.065	2	0.063	5
	4*	0.113	0.115	0.114			
A1809	30^{b2}	0.073	0.084	0.080	52	0.079	7
A2040	37	0.041	0.050	0.046	10	0.034	3
					21	0.046	3
A2048	7	0.037	0.042	0.040			
	25	0.094	0.103	0.097	1	0.095	5
A2052	35	0.030	0.045	0.035	61	0.035	9
A2353	24	0.117	0.125	0.121			
A2354	4	0.038	0.039	0.038			
	5	0.088	0.093	0.090			

Table 6. (continued)

ACO	N_z	z_{min}	z_{max}	$\langle z \rangle$	Literature		
					N_z	$\langle z \rangle$	ref.
A2361	24	0.059	0.063	0.061	2	0.061	5
	4*	0.200	0.203	0.201			
A2362	17	0.060	0.064	0.061	2	0.061	5
	4	0.131	0.134	0.133			
A2383	5	0.057	0.061	0.058			
	4	0.113	0.118	0.116			
	6	0.129	0.132	0.130			
A2401	23	0.054	0.061	0.057			
	5	0.092	0.095	0.093			
A2426	11^{m1}	0.086	0.089	0.088			
	15^{m2}	0.093	0.102	0.098			
A2436	4	0.056	0.061	0.058			
	14	0.087	0.095	0.091			
A2480	11	0.067	0.077	0.072		0.071	4
A2500	12	0.077	0.080	0.078			
	13	0.087	0.092	0.090			
	4	0.172	0.174	0.173			
A2502							
A2569	36	0.077	0.085	0.081			
A2644	4	0.060	0.061	0.060			
	12	0.068	0.070	0.069			
	7	0.133	0.135	0.134			
A2715	7	0.054	0.060	0.055			
	7	0.096	0.098	0.098			
	14	0.111	0.120	0.114			
A2717	40	0.042	0.052	0.049	33	0.049	8
	5	0.072	0.073	0.073			
A2734	5	0.026	0.027	0.026			
	83	0.054	0.067	0.062		0.063	4
	4	0.119	0.120	0.119			
	6*	0.137	0.141	0.141			
A2755	22	0.091	0.101	0.095		0.095	4
	10	0.117	0.124	0.121			
A2764	19	0.066	0.076	0.071		0.064	10
A2765	16^{m1}	0.076	0.083	0.080			
	4^{m2}	0.088	0.093	0.090			
A2778	7	0.075	0.079	0.077			
	17^{m1}	0.097	0.108	0.102		0.103	4
	10^{m2}	0.115	0.121	0.119		0.119	4
A2799	36	0.060	0.067	0.063		0.062	4
A2800	34	0.059	0.067	0.064			
A2819	49^{m1}	0.071	0.078	0.075			
	43^{m2}	0.082	0.090	0.087		0.087	4
	4	0.106	0.108	0.106			
	4	0.131	0.137	0.133			
	13	0.157	0.163	0.160			
A2854	22	0.060	0.064	0.061			
A2871	14^{m1}	0.112	0.116	0.114			
	18^{m2}	0.120	0.130	0.122			
A2911	7	0.020	0.022	0.020			
	31	0.075	0.086	0.081		0.079	4
	4	0.130	0.133	0.131			
A2915	4*	0.086	0.087	0.086			

Table 6. (continued)

ACO	N_z	z_{min}	z_{max}	$\langle z \rangle$	Literature		
					N_z	$\langle z \rangle$	ref.
A2923	5	0.016	0.019	0.017			
	16	0.071	0.074	0.071			
	4	0.127	0.130	0.128			
A2933	9	0.090	0.094	0.093			
A2954	6	0.056	0.057	0.057			
	5	0.125	0.127	0.126			
A3009	12	0.063	0.070	0.065		0.075	4
A3093	5	0.063	0.067	0.064		0.064	4
	22	0.080	0.086	0.083			
	6	0.113	0.118	0.115			
A3094	69	0.063	0.075	0.068			
	5	0.106	0.108	0.108			
	12	0.136	0.143	0.139			
A3108	7	0.060	0.063	0.063			
	5*	0.081	0.082	0.082			
A3111	35	0.074	0.084	0.078		0.080	4
A3112	77	0.059	0.082	0.075		0.076	4
	4	0.090	0.092	0.090			
	14	0.128	0.140	0.132			
A3122	92	0.055	0.070	0.064			
	8	0.114	0.120	0.117			
	10	0.148	0.152	0.150			
A3128	12*	0.039	0.047	0.039			
	158	0.051	0.071	0.060	43	0.059	8
	11*	0.075	0.078	0.077			
	4	0.106	0.108	0.107			
A3141	15	0.101	0.109	0.105		0.107	4
A3142	12^{b2}	0.062	0.069	0.066			
	21	0.096	0.107	0.103		0.103	4
A3144					16	0.045	4
A3151	38	0.059	0.072	0.068		0.068	4
A3158	105	0.052	0.067	0.059		0.058	10
	4*	0.072	0.074	0.074			
	4*	0.101	0.102	0.102			
A3194	32	0.093	0.102	0.097		0.098	4
A3202	27	0.066	0.072	0.069			
A3223	81	0.054	0.075	0.060		0.063	4
	8	0.109	0.111	0.110			
	8	0.135	0.140	0.137			
A3264	5	0.095	0.099	0.098			
A3301	5	0.053	0.057	0.054			
A3341	64	0.034	0.043	0.038		0.037	4
	15	0.075	0.082	0.078			
	18	0.112	0.117	0.115			
	7	0.130	0.134	0.131			
	5	0.151	0.154	0.154			
A3354	4	0.035	0.037	0.036			
	5^{m1}	0.042	0.044	0.044			
	58^{m2}	0.055	0.062	0.059			
	4	0.079	0.083	0.082			
	6	0.115	0.119	0.118			
	5	0.132	0.135	0.135			
	5	0.144	0.146	0.145			
	5	0.160	0.167	0.164			
	7	0.194	0.197	0.195			

Table 6. (continued)

ACO	N_z	z_{min}	z_{max}	$\langle z \rangle$	Literature		
					N_z	$\langle z \rangle$	ref.
A3365	32	0.088	0.101	0.092			
A3528	28	0.047	0.058	0.054			
	9	0.069	0.077	0.073			
A3558	4	0.030	0.033	0.032			
	75	0.040	0.056	0.048	267	0.048	11
A3559	7	0.013	0.015	0.014			
	39	0.043	0.050	0.047			
	6	0.072	0.078	0.077			
	11	0.110	0.116	0.113			
A3562	118	0.035	0.055	0.048			
A3651	79	0.053	0.065	0.060			
	5	0.100	0.101	0.101			
A3667	103	0.046	0.065	0.056	122	0.055	12
	5	0.097	0.103	0.099			
A3677	8	0.086	0.096	0.091			
A3682	10^{b2}	0.086	0.093	0.092			
A3691	33	0.081	0.094	0.087			
A3693	16	0.088	0.094	0.091			
	9	0.120	0.129	0.124			
A3695	81	0.082	0.099	0.089			
	7	0.130	0.132	0.131			
A3696	12^{b2}	0.086	0.092	0.088			
A3703	18	0.070	0.075	0.074		0.071	10
	13	0.089	0.098	0.091			
A3705	4	0.047	0.048	0.047			
	29	0.084	0.097	0.090	40	0.090	8
A3733	41	0.033	0.043	0.039	17	0.046	4
A3744	71	0.034	0.049	0.038			
	5	0.062	0.067	0.065			
A3764	38	0.072	0.084	0.076			
A3781	4	0.057	0.058	0.057			
	4	0.071	0.074	0.073			
A3795	13	0.086	0.091	0.089			
A3799	10	0.043	0.047	0.045			
A3806	9	0.053	0.055	0.054			
	99	0.065	0.086	0.076			
	4	0.137	0.139	0.138			
A3809	94	0.057	0.072	0.062		0.062	4
	4	0.090	0.091	0.091			
	10	0.108	0.112	0.110			
	11	0.139	0.148	0.141			
	4*	0.152	0.156	0.152			
A3822	4*	0.037	0.040	0.039			
	4	0.052	0.053	0.052			
	84	0.066	0.083	0.076			
	4	0.099	0.105	0.102			
A3825	61	0.067	0.080	0.075			
	17^{m1}	0.097	0.112	0.104			
	4^{m2}	0.116	0.121	0.119			
A3827	20	0.093	0.108	0.098		0.099	10
A3864	6	0.075	0.079	0.077			
	32	0.095	0.109	0.102			

Table 6. (continued)

ACO	N_z	z_{min}	z_{max}	$\langle z \rangle$	Literature		
					N_z	$\langle z \rangle$	ref.
A3879	5	0.050	0.051	0.050			
	45	0.059	0.074	0.067		0.068	4
	7	0.095	0.099	0.097			
	5	0.127	0.131	0.130			
A3897	10	0.071	0.077	0.073			
A3921	32	0.086	0.101	0.094		0.096	4
	4	0.133	0.136	0.134			
A4008	27	0.052	0.057	0.055			
	7	0.102	0.114	0.107			
A4010	30	0.091	0.100	0.096			
A4053	9	0.049	0.052	0.050			
	17	0.066	0.075	0.072			

Notes: Systems adjacent in redshift that are indicated by $m1$, $m2$, $m3$ etc., are merged into one group by the method of ZHG. Systems marked by $b2$ or $b3$ are broken up in two or three groups respectively by the ZHG method. An $*$ indicates that the system is not found by the ZHG method.

References: 1. Fabricant et al. (1993); 2. Proust et al. (1992); 3. Zabludoff et al. (1990); 4. Dalton et (1994); 5. Struble & Rood (1991); 6. Capelato et al. (1991); 7. Hill & Oegerle (1993); 8. Colless & Hewett (1987); 9. Malumuth et al. (1992); 10. Andernach (priv. comm.) 11. Bardelli et al. (1994); 12. Sodré et al. (1992)

perhaps most obviously, the properties of the dominant groups will be studied. This involves the determination and analysis of the distribution of velocity dispersions for a complete, volume-limited sample of rich clusters (Mazure et al. 1995), as well as the detailed analysis of the structure of the phase-space of the individual clusters. Another aspect of our dataset that is immediately apparent from Fig. 7 concerns the information it contains on the large-scale structure in the Universe. Although it has become customary to discuss the redshift distributions in very deep, randomly positioned pencil beams for that purpose (see e.g. Broadhurst et al. 1990), our 107 pencil beams in the directions of rich clusters can give complementary information on the characteristics of large-scale structure. Finally, the comparison between the dynamics of galaxies with and without emission lines that could be detected in our observations is interesting and in progress.

The above list of possible uses that our data can be put to is not meant to be complete. Clearly, there is interest in comparing the galaxy kinematics with information from X-ray imaging and spectroscopy. It will also be very interesting to compare our data to the predictions of sufficiently realistic N-body simulations of clusters, in particular to those in which the modeling of the formation and evolution of galaxies is attempted (e.g. by Van Kampen, 1994 and 1995).

We are still working on several questions for which the present dataset provides unique new information. The entire dataset will however be made public in the near future.

In this paper we have concentrated on the properties of our dataset. We have described the methods that we used to generate it, and we have discussed its reliability which, at an overall value of 0.98 for the 5634 redshifts in the catalogue, is quite satisfactory. Finally, we have used our data to study the effects of field contamination and superposition, for our sample of nearby and rich Abell clusters. We conclude that, for such a subset of the ACO catalogue, these effects are probably sufficiently small that they do not preclude its use for meaningful statistical studies.

Acknowledgements. We gratefully acknowledge the support given to this project by ESO, first by accepting it as a Key-programme, and secondly by allocating the large amount of telescope time without which this project would not have been possible. We extend special thanks to G. Avila, who has been very helpful in many aspects of the observational program, such as the production of the aperture plates, and the optimization of the performance of the Optopus multi-fibre system. At the 3.6-m telescope we were very ably assisted by G. Roman, A. Alvarez, M. Bahamondes, and L. Ramirez. PK acknowledges very useful discussions with R.S. Le Poole on several aspects of the data analysis. The cooperation between the members of the project was financially supported by the following organizations: INSU, GR Cosmologie, Univ. de Provence, Univ. de Montpellier (France), CNRS-NWO (France and the Netherlands), Leiden Observatory, Leids Kerkhoven-Bosscha Fonds (the Netherlands), Univ. of Trieste, Univ. of Bologna (Italy), the Swiss National Science Foundation, the Ministerio de Educacion y Ciencia (Spain), CNRS-CSIC (France and Spain) and by the EC HCM programme. Finally, we acknowledge several useful comments of the referee, L. Guzzo.

Appendix A: the estimation of the reliability of our redshifts

Here we present some details of the evidence on which we based our estimates of the reliability of the redshifts. All the evidence is empirical and based on independent multiple measurements. First, we use two sets of consecutive Optopus exposures (with only the CCD read-out in between), which were reduced separately, to estimate the S/N-ratio in the correlation function above which the reliability is essentially 1.0. Then we use all available pairs of multiple measurements of *accepted* absorption-line redshift estimates to deduce the actual reliability of the redshifts in our catalogue. A similar analysis is made for the multiple measurements of emission-line redshifts. Finally, we use all galaxies for which both an (independently measured) absorption- and emission-line redshift were obtained to refine our estimates of the reliability of the different types of redshift estimate.

The two sets of consecutive double exposures, which were reduced completely separately (contrary to the normal procedure for double exposures, which were combined before calibration and reduction), with 46 and 47 spectra respectively, yielded 93 pairs of redshifts. Of these, 23 were found to be discordant, and in all discordant pairs at least one of the redshifts had a S/N-ratio of the correlation peak less than 3.0. The statistics in Table 7 shows that for a S/N-ratio ≥ 3.0 the reliability of a redshift estimate is essentially 1.0, while for S/N-ratios < 3.0

Table 7. The reliability of the redshifts as inferred from blindly accepted estimates in 2 consecutive exposures.

S/N_1	S/N_2	# pairs	concordant	discordant
$\geq$3.0	$\geq$3.0	52	52	0
$\geq$3.0	<3.0	10	7	3
<3.0	<3.0	31	11	20
total pairs:		93	70	23

Table 8. The reliability of the redshifts as inferred from pairs of estimates accepted after inspection of correlation function and spectrum

S/N_1	S/N_2	# pairs	concordant	discordant
$\geq$3.0	$\geq$3.0	265	265	0
$\geq$3.0	<3.0	84	80	4
<3.0	<3.0	43	39	4
total pairs:		392	384	8

Table 9. The reliability of redshift estimates based on emission lines.

#-lines$_1$	#-lines$_2$	# pairs	concordant	discordant
multiple	multiple	30	30	0
multiple	single	14	12	2
single	single	3	3	0
total pairs:		47	45	2

Table 10. Agreement between absorption- and emission-line redshifts.

z_{abs}	z_{emi}	# pairs	concordant	discordant
S/N $\geq$ 3.0	$\geq$ 2 lines	162	159	3
	1 line	162	130	32
S/N < 3.0	$\geq$2 lines	230	210	20
	1 line	112	87	25
total pairs:		666	586	80

the average reliability is of the order of 0.60$\pm$ 0.05. Note that for this analysis *all* redshift pairs were used (i.e. the plausibility of individual redshift estimates was not judged), as we are interested here in the influence of the noise in the correlation function. From Table 7 we conclude that the S/N-ratio below which the reliability of a redshift estimate starts to decline (fairly rapidly) is about 3.0. In the following we will therefore use this value to separate redshifts with identical high reliability (equal to 1.0) from redshifts with lower reliabilities (between 0.0 and 1.0).

Rather than accept all redshift estimates blindly (as was done for the statistics in Table 7), each and every redshift estimate was checked for plausibility by simultaneous visual inspection of the spectrum and the correlation function. The reliability of essentially 1.0 for the S/N $\geq$ 3.0 redshifts was confirmed by the visual inspection and none of these redshifts was rejected. However, quite a few of the S/N < 3.0 redshifts were judged very improbable and rejected. Therefore, the reliability of the *accepted* redshifts with S/N < 3.0 is very likely to be much higher than the value of 0.6 implied by the data in Table 7.

We have used the multiple measurements of redshifts to estimate the actual reliability of the *accepted* S/N < 3.0 redshifts. For 360 galaxies at least two independent redshift estimates were accepted; in 22 cases three, and in 5 cases even four redshifts were available for a given galaxy. Thus, we have 392 independent pairs for which we can carry out the same analysis as for the 97 pairs in the two double exposures discussed above. In Table 8 we show the statistics for the 392 pairs. From these we conclude that the reliability of the S/N-ratio $\geq$ 3.0 redshifts is indeed 1.00. The average reliability of the *accepted* S/N-ratio < 3.0 redshifts turns out to be considerably higher than 0.6, namely about 0.95. This illustrates the great value of the visual inspection, which seems to have reduced the fraction of erroneous redshifts by almost 90 per cent.

The reliability of the emission-line redshifts was estimated in an analogous way. We have 47 independent pairs of emission-line redshifts. It seems quite natural to distinguish estimates based on one line only (whether it be OII, Hβ or OIII) from estimates based on a combination of at least two lines. In Table 9 we show the rather limited statistics. As a first approximation, we conclude that emission-line redshifts based on at least two lines have a reliability of essentially 1.00, while those based on a single line (which does not need to be the OIII doublet) have a reliability of 0.85 $\pm$ 0.10.

Finally, we have analyzed the results for the 666 galaxies with both an absorption- and an emission-line redshift. In Table 10 we show the statistics of the concordant and discordant pairs. We interpret the data in this Table as follows. Accepting the previous result that the reliability of the absorption-line redshifts with S/N $\geq$ 3.0 is 1.00, we conclude from the upper half of the Table that the reliability of the 'multiple' emission-line redshifts is 0.98. Similarly, the single emission-line redshifts appear to have a reliability of about 0.80. Note that both conclusions are completely consistent with the earlier estimates. The lower half of the Table then tells one that the reliability of the accepted S/N < 3.0 absorption-line redshifts is 0.95 (again confirming the earlier, completely independent, estimate). The multiple-line emission-line redshifts have a reliability of 0.97, and the single-line emission-line redshifts of 0.81. All these reliability estimates are believed to be accurate to between 1 and 2 per cent.

References

Abell, G.O., 1958, ApJS, 3, 211
Abell, G.O., Corwin, H.G., Olowin, R.P., 1989, ApJS, 70, 1 (ACO)
Abt, H.A., Biggs, E.S., 1972, Bibliography of Stellar Radial Velocities, Latham Process Corp., New York
Avila, G., D'Odorico, S., Tarenghi, M., Guzzo, L., 1989, ESO Messenger, No. 55, p. 62
Bardelli, S., Zucca, E., Vettolani, et al. 1994, MNRAS, 267, 665
Beers, T.C., Forman, W., Huchra, J.P., Jones, C., Gebhardt, K., 1991, AJ, 102, 1581
Biviano, A., Girardi, M., Giuricin, G., Mardirossian, F., Mezzetti, M., 1992, ApJ, 396, 35
Briel, U.G., Henry, J.P., 1993, A&A, 278, 390
Broadhurst, T.J., Ellis, R.S., Koo, D.C., Szalay, A.S., 1990, Nature, 343, 726
Capelato, H.V., Mazure, A., Proust, et al. 1991, A&ASS, 90, 355
Chincarini, G., Tarenghi, M., Bettis, C., 1981, A&A, 96, 106
Colless, M., Hewett, P., 1987, MNRAS, 224, 453
Colless, M., 1989, MNRAS, 237, 799
Dalton, G.B., Efstathiou, G., Maddox, S.J., Sutherland, W.J., 1992, ApJL, 390, L1
Dalton, G.B., Efstathiou, G., Maddox, S.J., Sutherland, W.J., 1994, MNRAS, 269, 151
De Vaucouleurs, G., De Vaucouleurs, A., Corwin, H.G. Jr., et al. 1991, Third Reference catalogue of Bright Galaxies, ed. Springer-Verlag
De Vries, C.P., 1987, PhD thesis, Leiden
Dressler, A., Shectman, S.A., 1988, AJ, 95, 284
Faber, S.M., Dressler, A., 1977, AJ, 82, 187
Fabricant, D., Beers, T.C., Geller, M.J., et al. 1986, ApJ, 308, 530
Fabricant, D., Kurtz, M.J., Geller, M., et al. 1993, AJ, 105, 788
Guzzo, L., Collins, C.A., Nichol, R.C., Lumsden, S.L., 1992, ApJ, 393, L5
den Hartog, R.H., Katgert, P., 1995, submitted to MNRAS
Heydon-Dumbleton, N.H., Collins, C.A., MacGillivray, H.T., 1989, MNRAS, 238, 379
Hill, J.M., and Oegerle, W.R., 1993, AJ, 106, 831
Le Fèvre,O., Bijaoui, A., Mathez, G., Picat, J.P., Lelievre, G., 1986, A&A, 154, 92
Lissandrini, C., Cristiani, S., La Franca, F., 1994, PASP, 106, 1157
Lucey, J.R., 1983, MNRAS, 204, 33
Lucey, J.R., Dickens, R.J., Mitchell, R.J., Dawe, J.A., 1983, MNRAS, 203, 545
Lumsden, S.L., Nichol, R.C., Collins, C.A., Guzzo, L., 1992, MNRAS, 258, 1
Lund, G., 1986, ESO Operating Manual No. 6
Maddox, S.J., Sutherland, W.J., Efstathiou, G., Loveday, J., 1990, MNRAS, 243, 692
Malumuth, E.M., Kriss, G.A., Van Dyke Dixon, W., Ferguson, H.C., Ritchie, C., 1992, AJ, 104, 495
Materne, J., Hopp, U., 1983, A&A, 124, L13
Mazure, A., Katgert, P., Den Hartog, R.H., et al. 1995, TO BE FILLED IN BY EDITOR AANDA
Pierre, M., Böhringer, H., Ebeling, H., et al. 1994, A&A, 290, 725
Pisani, A., 1993, MNRAS, 265, 706
Proust, D., Quintana, H., Mazure, A., et al. 1992, A&A, 258, 243
Sarazin, C., 1986, Rev. Mod. Phys., 58,1
Sodré, L., Capelato, H.V., Steiner, J.E., Proust, D., Mazure, A., 1992, MNRAS, 259, 233
Struble, M.F., Rood, H.J., 1991, ApJS, 77, 363
Sutherland, W., 1988, MNRAS, 234, 159
Swaans, L., 1981, PhD thesis, Leiden
Teague, P.F., Carter, D., Gray, P.M., 1990, ApJS, 72, 715
Tonry, J., Davis, M., 1979, AJ, 84, 1511
Van Haarlem, M.P., Le Poole, R.S., Katgert, P., Tritton, S., 1991, MNRAS, 255,
Van Kampen, E., 1994, PhD thesis, Leiden Observatory
Van Kampen, E., 1995, MNRAS, 273, 295
West, M.J., Dekel, A., Oemler, A., 1987, ApJ, 316, 1
White, S.D.M., 1991, in *Large Scale Structures and Peculiar Motions in the Universe*, eds. Latham, D.W. & Da Costa, L.N., ASP, p285
White, S.D.M., 1992, in *Clusters and Superclusters of Galaxies*, ed. A.C. Fabian, NATO ASI Series C366, Kluwer Acad. Publ. Dordrecht
Zabludoff, A.I., Huchra, J.P., Geller, M.J., 1990, ApJS, 74, 1 (ZHG)
Zabludoff, A.I., Geller, M.J., Huchra, J.P., Vogeley, M.S., 1993, AJ, 106, 1301 (ZHGV)
Zucca, E., Zamorani, G., Scaramella, R., Vettolani, G., 1993, ApJ, 407, 470

This article was processed by the author using Springer-Verlag LaTeX A&A style file version 3.